EUROPEAN COMMISSION

Community Research

SEVENTH FRAMEWORK PROGRAMME

ARCHER

Collaborative Project (CP)

Co-funded by the European Commission under the Euratom Research and Training Programme on Nuclear Energy within the Seventh Framework Programme

Grant Agreement Number : 269892

Start date : 01/02/2011 Duration : 48 Months

www.archer-project.eu

Archer

Advanced Reactor for Cogeneration of Heat & Electricity-R&D

Fuel performance modelling of HFR-EU1 under normal and off normal conditions

Authors : Karl Verfondern (FZJ), Laurent Gauthier (AREVA)

ARCHER - Contract Number: 269892
Advanced High-Temperature Reactors for Cogeneration of Heat and Electricity R&D
EC Scientific Officer: Dr. Panagiotis Manolatos

Document title	Fuel performance modelling of HFR-EU1 under normal and off normal conditions
Author(s)	Karl Verfondern (FZJ), Laurent Gauthier (AREVA)
Number of pages	72
Document type	Deliverable
Work Package	WP 32
Document number	D32.41
Issued by	FZJ
Date of completion	18/03/2015
Dissemination level	Confidential, only for members of the consortium (including the Commission Services).

Summary

Within the frame of the ARCHER project, R&D activities have been starting to evaluate the irradiation experiment HFR-EU1. The study presented here is dealing with the calculations of fuel performance and metallic fission product release during irradiation based on the operational data available up to now, and also includes a comparison with predictive calculations from the past.

Approval

Date	By
19/03/2015	Mathias LAURIE
19/03/2015	Mathias LAURIE
20/03/2015	Steven KNOL

Distribution list

Name	Organisation	Comments
P. Manolatos	EC DG RTD	Through the EC participant portal
All beneficiaries	ARCHER	Through the private online workspace

Table of contents

1 Introduction

Within the European irradiation testing program for HTGR fuel, the so-called HFR-EU1 irradiation experiment was initiated with the goal to explore the performance limits of the presently existing German and Chinese high-quality fuel [Laurie 2010a].

The objective of the irradiation experiment HFR-EU1 [Marmier 2008] was the exploration of the potential for high performance and high burnup of both the existing German fuel spheres and newly produced Chinese fuel spheres for advanced applications. The fuel irradiation was conducted in two phases between 2006 and 2010 under defined conditions to high burnups. The spheres will later be transported to the ITU, Karlsruhe, for further postirradiation examinations (PIE) including heatup simulation testing in the KÜFA-II furnace to allow further insight into fuel performance and fission product release behavior.

The experiment is planned to be completed with further extensive PIE at NRG Petten and JRC-ITU in Karlsruhe including KÜFA tests. Dismantling, PIE, transport and safety tests are planned to take place as part of the ARCHER project [Groot 2010].

TABLE 1: Labeling of fuel elements in the experiment HFR-EU1.

Project description of fuel elements	Petten description of fuel elements
HFR-EU1/1	INET 1
HFR-EU1/2	INET 2
HFR-EU1/3	AVR 1
HFR-EU1/4	AVR 2
HFR-EU1/5	AVR 3

2 HFR-EU1 Irradiation

2.1 Fuel

There were totally five spherical fuel element samples to be tested in this experiment, each of them 60 mm in diameter with LEU UO_2 TRISO coated particles. The three German pebbles were of type AVR GLE-4 produced as AVR reload 21-2 in October 1987. They were manufactured by HOBEG. The two Chinese pebbles were manufactured by INET and taken from the fuel production for the operation of the HTR-10 test reactor. Fuel characteristics are listed in Table 2.

TABLE 2: Characteristic data[a] of AVR GLE-4 and INET spherical fuel elements with LEU TRISO UO_2 fuel particles as loading for the experiment HFR-EU1.

	AVR GLE 4-2 spheres	INET spheres
Diameter [mm]	60	60
Matrix graphite grade	A3-3	A3-3
Heavy metal loading [g/FE]	6.0	5.02
U-235 contents [g/FE]	1.00	0.858
No. of particles per sphere	9560	8500
Volume packing fraction [%]	6.2	5.0
Defective SiC layers [U/U_{tot}]	7.8×10^{-6}	2.3×10^{-7}
Coated particle batch	HT 385-393, 395-404, 406-423	V000802
UO_2 kernel diameter [µm]	502	490
Enrichment [U-235 wt.%]	16.76	17.08
Coating thickness [µm]		
Buffer	95	98
Inner PyC	41	42
SiC	35	38
Outer PyC	40	41

a as used in the calculations

2.2 Irradiation Setup

The design of HFR-EU1 is based on previous experience of HTGR fuel irradiations within the European Union, namely HFR-P4, HFR-K5, HFR-K6 and SiC coated graphite spheres. The five pebbles (plus a couple of mini-samples with 10 coated particles each) were tested in a standard re-usable REFA-172 rig. The fuel spheres were placed in two separate capsules, one for the three German spheres, the other one for the two Chinese spheres. These sample holders equipped with separate gas lines represent the 1st containment containing graphite cups (SGL R6650) to hold the pebbles in place. The REFA-172 rig forms the 2nd containment. A schematic drawing is shown in Fig. 1 [Laurie 2010a].

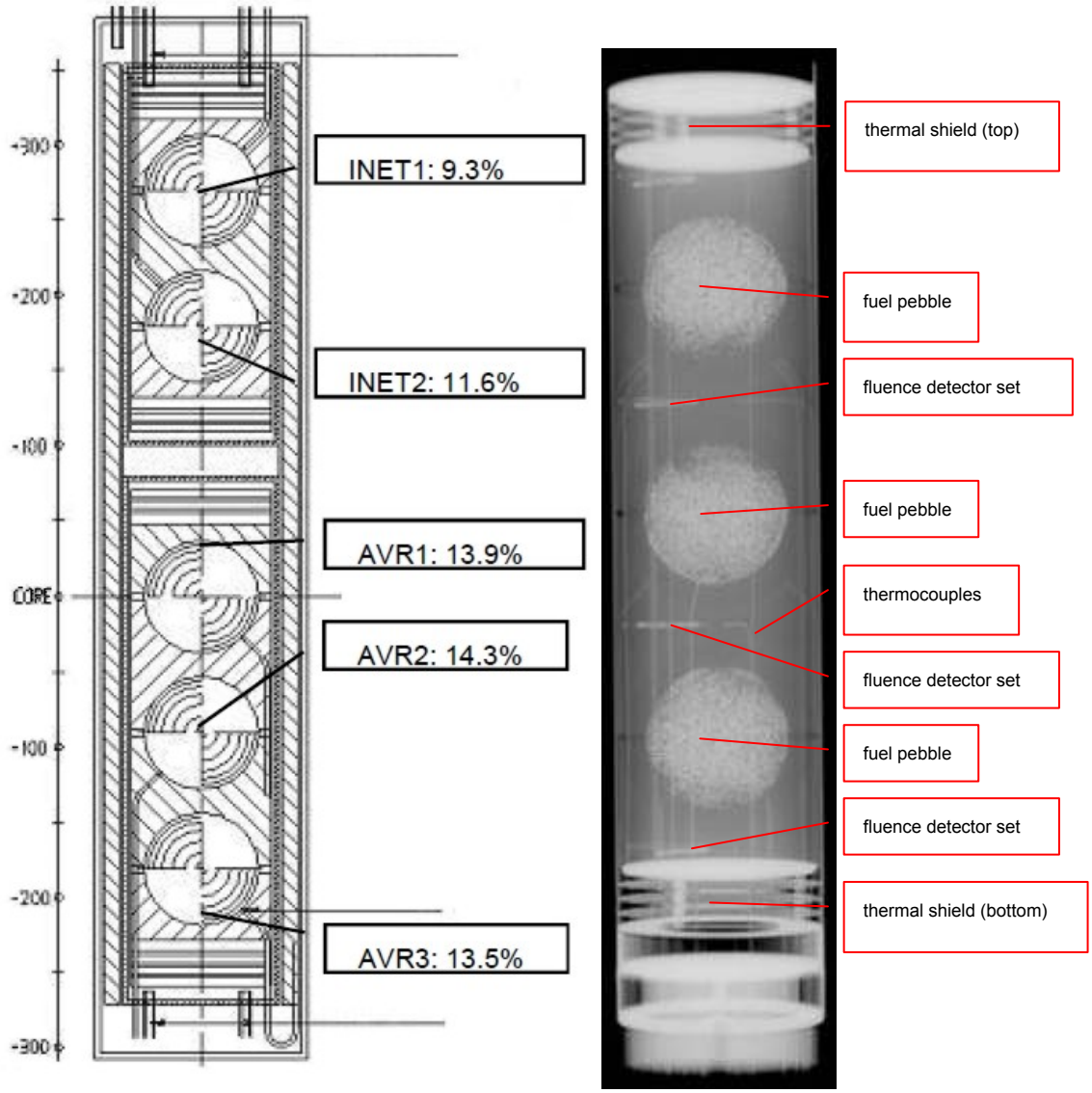

FIGURE 1: Cross-section of the HFR-EU1 sample holder with upper Capsule 1 containing two Chinese spheres and lower Capsule 2 containing three German spheres with final burnups in boxes (left); pre-irradiation X-ray of German capsule (right).

Nuclear instrumentation includes 12 neutron fluence detector sets, 4 self-powered neutron detectors and 4 gamma scan wires. The heat generated by fission and photons dissipates mainly radially through the materials by conduction and through the gas gaps by conduction/radiation to the outside containment, which is cooled by primary cooling water. The temperature of the fuel surface was controlled by adjusting the He/Ne blend in both the 1st and 2nd containments. This temperature adjustment was required to compensate for changes of time and fluence dependent operating parameters such as fission power depletion (burnup), dimensional changes of specimen assembly (graphite shrinkage), changes in thermal conductivity and thermal expansion, changes in nuclear characteristics from cycle to cycle, and movements of reactor control rods.

This experiment was connected to a new gas handling facility [Laurie 2010a, Laurie 2010b] that enabled continuous instead of batchwise fission gas release analysis. The 1st and 2nd containments were continuously purged with a constant gas flow of 50 ml/min during the whole irradiation which facilitated temperature adjustment and gas sampling. This setup with a higher gas pressure in the 2nd containment enabled permanent integrity

surveillance of the 1st containment. Cycle-by-cycle turning of the experiment by 180° was applied to flatten neutron fluence and radial burnup gradients across pebbles.

The experiment was designed such that despite the decrease in power with time the desired surface temperature could be kept as constant as possible for all pebbles over the entire irradiation. This was achieved by sizing the gas gaps between graphite cups and 1st containment tube and 1st and 2nd containment tubes such that a suitably adjusted He/Ne blend enabled obtaining the required pebble temperatures. HFR-EU1 was conducted with constant surface temperature with the consequence that power depletion with burnup continuously decreased the central temperatures during the experiment.

2.3 Irradiation Conduction

HFR-EU1 was initially designed to be conducted at a relatively slow pace (lower neutron flux and fission power) with an initially estimated 22 calendar months of irradiation time. However, the conversion of the HFR reactor from HEU to LEU finished only a few months before the start of the experiment required changes in the position of the experiment inside the reactor inducing significant power variations. The irradiation test was performed in two campaigns

- 12 cycles between Sep 2006 and Feb 2008; and
- 4 cycles between Oct 2009 and Feb 2010

totaling 445 equivalent full power days (efpd). The almost 2-years discontinuation of the test between the two campaigns was due to shutdown of the HFR reactor.

Thirty-four thermocouples (TC) were built into the experiment. They were supplied by Thermocoax and were of type N (Nicrosil/Nisil wires, MgO insulator, Inconel 600 sheath) with an outer diameter of 1.05 mm. The upper sample holder (INET fuel) was equipped with 14 thermocouples, while the lower one (AVR fuel) had 20. Already after 12 irradiation cycles, 4 out of the 14 INET and 16 of the 20 AVR TC provided physically impossible or unreliable signals. The experiment ended with 6 out of 14 damaged TC in the INET capsule and 18 out of 20 damaged TC in the AVR capsule (Table 3).

TABLE 3: Locations of installed thermocouples with red-marked numbers indicating those which eventually failed during the course of irradiation.

Location	TC #
Top Graphite INET	1, 2
INET.1	3, 4, 5, 6
Graphite between INET.1 and INET.2	7, 8
INET.2	9, 10, 11, 12
Bottom Graphite INET	13, 14
Top Graphite AVR	15, 16
AVR.1	17, 18, 19, 20
Graphite between AVR.1 and AVR.2	21, 22
AVR.2	23, 24, 25, 26
Graphite between AVR.2 and AVR.3	27, 28
AVR.3	29, 30, 31, 32
Bottom Graphite AVR	33, 34

Figure 2 shows the time-averaged fuel element surface temperatures for all 16 irradiation cycles without correction for thermal drift and neutron induced de-calibration of thermocouples [Laurie 2010a]. Typically, circumferential temperature differences of approx. 50°C were observed, mainly due to the unexpectedly strong axial flux buckling on the top of the capsule. These conditions allowed to stick to the 950°C target temperature for the German spheres, while that for the lower INET sphere (No. 4) was slightly reduced to 940°C. Still, the fuel surface temperatures were sensitive to HFR power fluctuations, experiment loading and control rod movements.

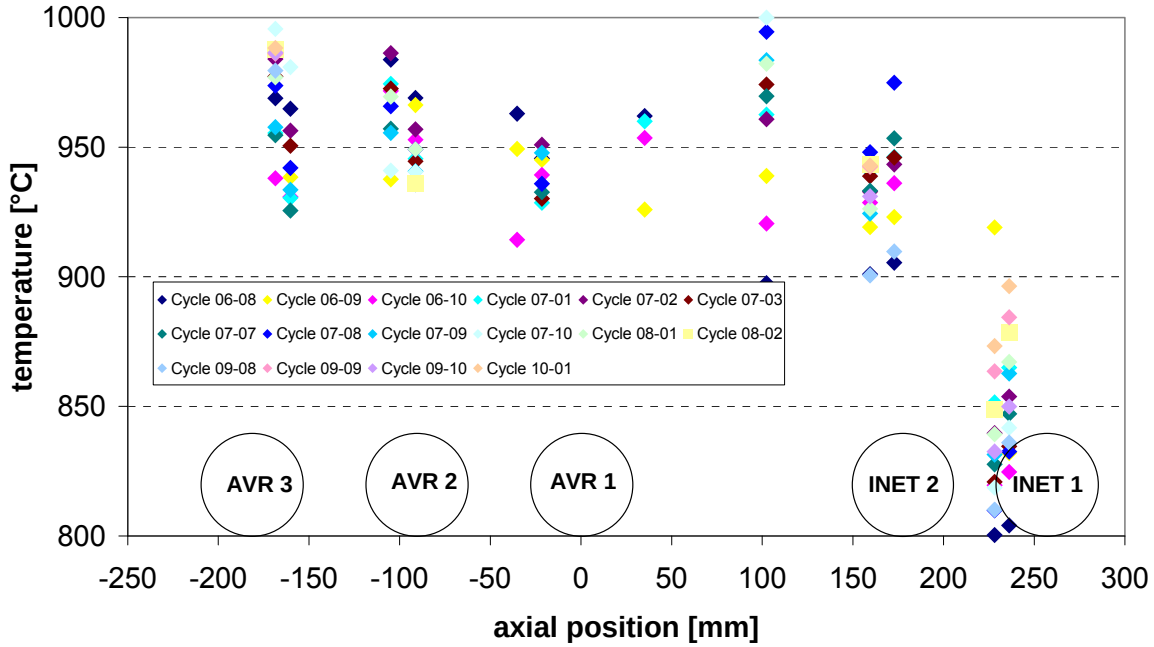

FIGURE 2: Cycle-averaged fuel element surface temperatures measured in irradiation rig.

The burnup shown in Fig. 3 has been pre-calculated for the HFR-EU1 experiment (capsule averaged). Later adjustments will be made once the burnup measurements of the pebbles and the analyses of gamma scan wires and fluence detectors will be available. During 445 efpd, the pre-calculated maximum burnup of 14.3% FIMA is expected for one of the German spheres with a fast neutron fluence of approximately 4.95×10^{25} n/m^2. The INET spheres have presumably achieved burnups of 9.28% FIMA and 11.7% FIMA, respectively.

Burnup data should be considered preliminary, until respective measurements planned at ITU, Karlsruhe, were made.

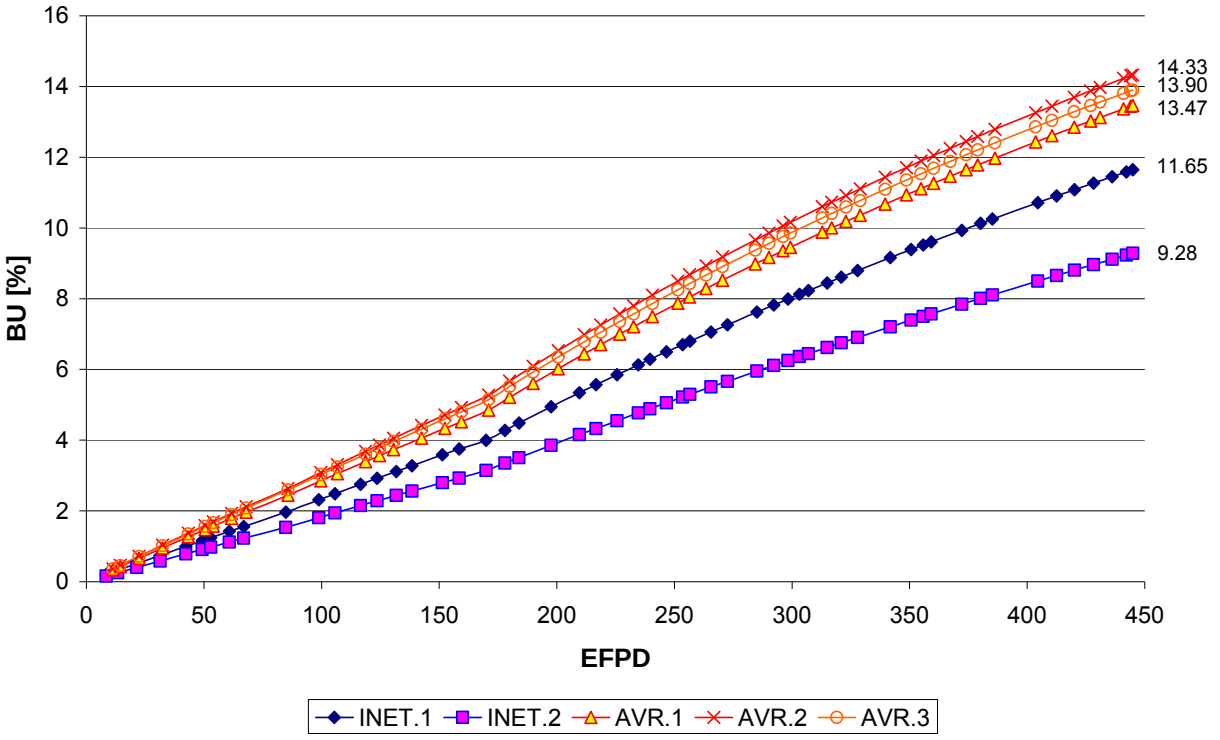

FIGURE 3: Burnup vs. irradiation time for all five HFR-EU1 pebbles.

2.4 Fission Gas Release Measurements in HFR-EU1

HFR-EU1 was conducted using a newly built gas handling station, the so-called "sweep loop facility", SLF [Laurie 2010b]. It provided all containments with variable gas blends for temperature control and enabled permanent surveillance of containment integrity as well as gas sampling for fission gas release measurements by gamma spectrometry. Gas sampling was in general performed once per week per capsule. Temperature was adjusted by mixing He and Ne while keeping the total gas flow rate constant, typically 50 ml/min. For gas sampling, the gas flows from the 1st containment were routed through a detachable grab sample with a volume of 100 cm^3. This grab sample was then removed from the glove box and placed on a multi-channel gamma spectrometer calibrated for the measurement of five different isotopes, namely ^{85m}Kr, ^{87}Kr, ^{88}Kr, ^{133}Xe, and ^{135}Xe. Of each sample, several measurements were made and the counts were corrected for decay to determine the specific isotope concentration in the purge gas at the moment of gas sampling. The statistical error of this measurement ranged between 4 and 9%. Together with the known gas flow, pressure and temperature, the fission gas release rate R from the two capsules could be determined and related to the birth rate B from neutronics calculations (error approx. 10%) thus yielding the characteristic R/B value which is considered a good health indicator of coated particle fuel.

At the end of irradiation, based on ^{85m}Kr, an R/B of approx. 8×10^{-8} for INET fuel (Fig. 4) and 2.5×10^{-7} for AVR fuel (Fig. 5) was measured [Laurie 2010a], which is at least two orders of magnitude lower than the R/B corresponding to a theoretical full fission gas release of a single particle in the capsules (which would be approx. 5.4×10^{-3} (@ 1000°C) and 8.4×10^{-3} (@ 1100°C) for the INET and AVR capsule, respectively). For comparison, in the earlier experiments HFR-K5 and HFR-K6, R/B values of 5×10^{-7} had been measured on fresh fuel. More recently and at very high temperature, HFR-EU1bis produced higher R/B of approx. 4×10^{-6} [Fütterer 2008, Groot 2010].

The result suggests that in none of the HFR-EU1 pebbles particle failure has occurred. Instead, the measured fission gas release probably originates from uranium and thorium impurities in the matrix graphite of the pebbles and in the graphite cups used to hold the pebbles in place. To validate this assumption, the same neutronic method used for the pebbles was applied to the graphite cups considering a probable graphite contamination of 50 wt-ppb of natural uranium and of 250 wt-ppb of thorium [Van der Merwe 2008]. Figure 6 shows the ratio of fission rate from contamination to the one from a single particle calculated up to 332 efpd [Laurie 2010a]. One can deduce from this figure that after 332 efpd, the contamination accounts for > 11% of one INET particle and > 22% of one AVR particle. Measured fission gas release must thus be higher than this value before one may conclude on full particle failure.

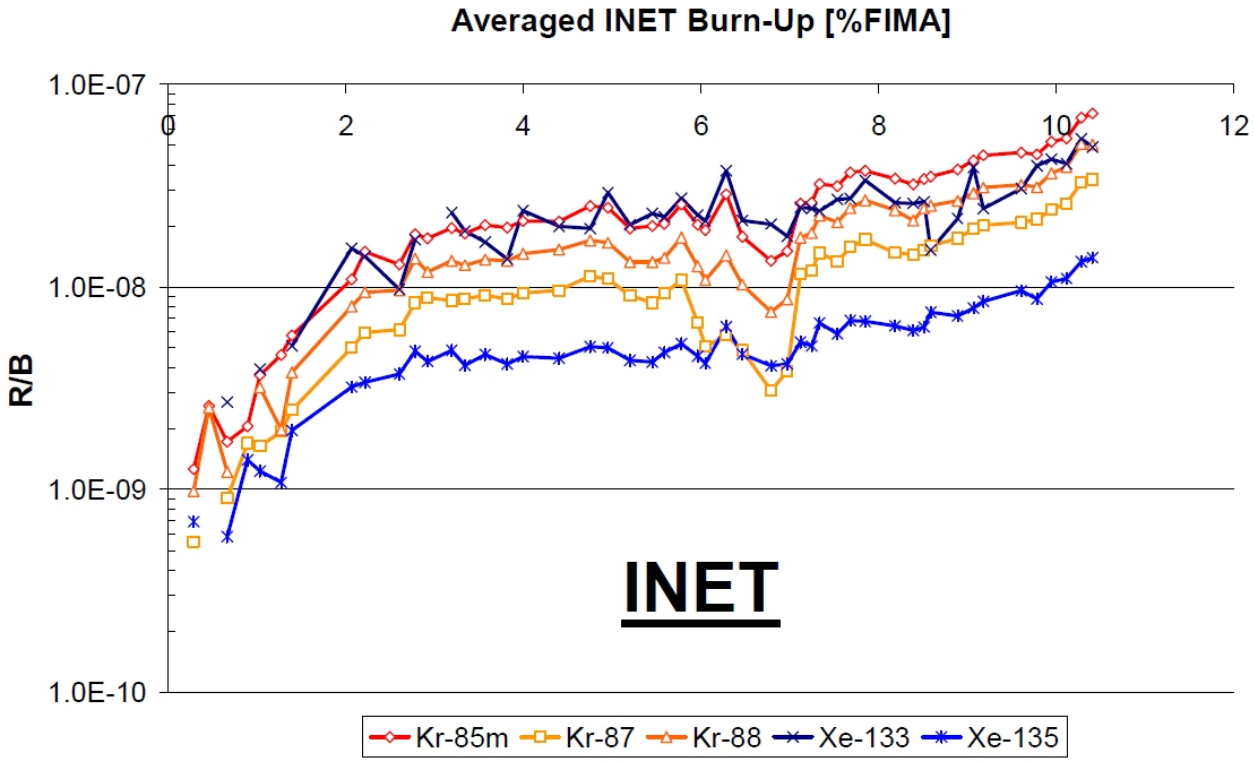

FIGURE 4: Measured R/B vs. burnup for INET spheres.

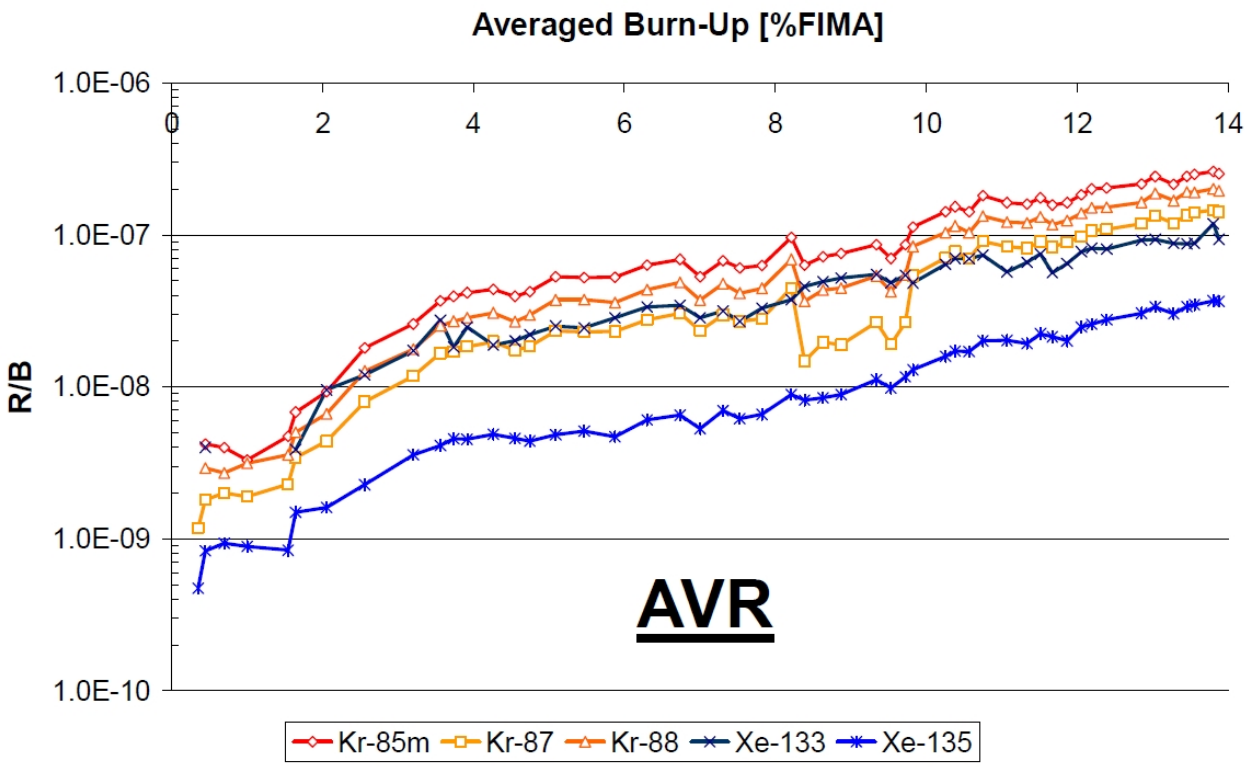

FIGURE 5: Measured R/B vs. burnup for AVR spheres.

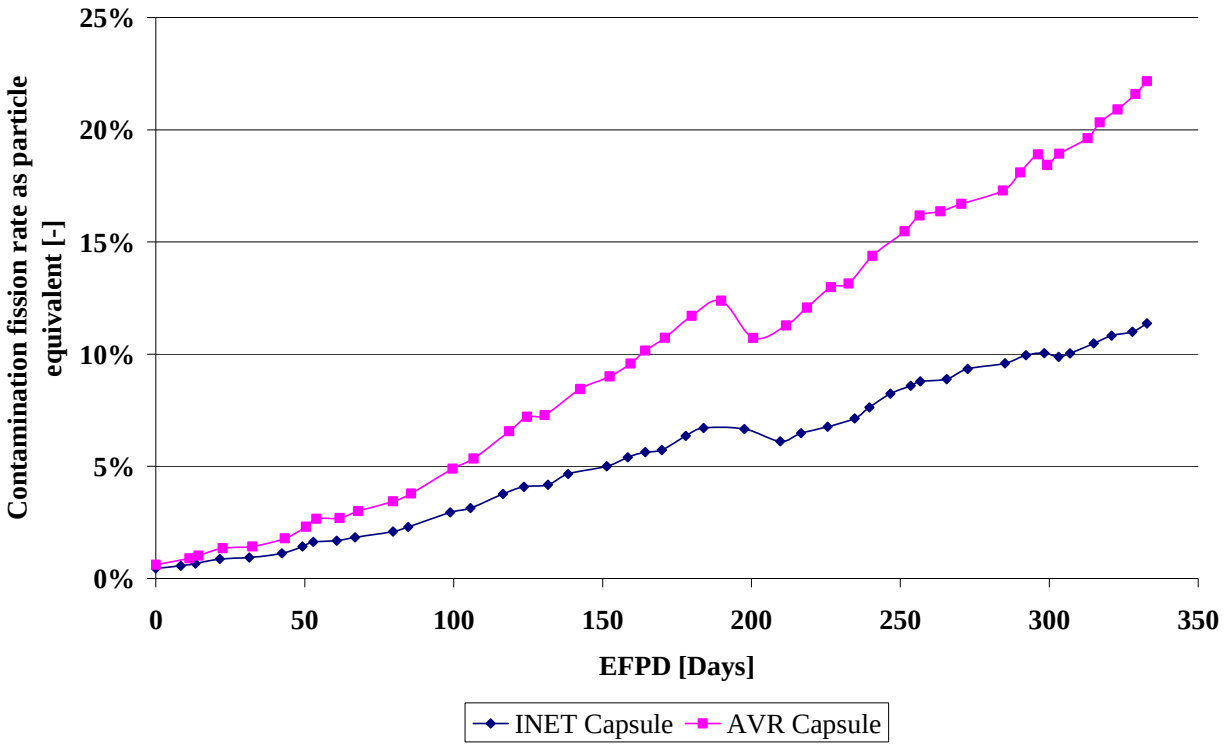

FIGURE 6: Relative significance of fission gas release from graphite contamination compared to a single fuel kernel.

3 Computational Methods

3.1 Computer Code PANAMA

The FZJ computer code PANAMA [Verfondern 1985] simulates the mechanical performance of TRISO coated fuel particles under given normal operation and accident conditions. The failure probability, Φ_p, which is of importance under the conditions of normal reactor operation and core heatup accidents for modular type HTGRs, is based on a pressure vessel model and includes a degradation effect on the SiC layer due to fission product corrosion.

In the pressure vessel model, the SiC layer represents the wall of a simplified pressure vessel, while all other layers are ignored. This pressure vessel is assumed to fail as soon as the stress induced in the SiC layer by the internal gas pressure, σ_t, exceeds the tensile strength of the SiC, σ_o. The probability for a pressure vessel failure of a particle is a function of time and temperature and can be described according to the Weibull equation:

$$\Phi_p(t,T) = 1 - \exp\left\{-\ln 2 * \left(\sigma_t / \sigma_o\right)^m\right\}$$

The tensile strength is a material parameter, whose mean value and statistical Weibull modulus, m, can be derived, e.g., from SiC ring crack tests [Bongartz 1976]. The SiC layer is weakened under irradiation. Its strength is assumed to decrease as a function of the fast neutron fluence as was derived from measurements on the German particle batch EO 1607.

The effect of fission product corrosive attack on the silicon carbide is transformed into a thinning of the SiC layer, i.e., the pressure vessel wall, at a volume corrosion rate $\dot{v}$ according to [Montgomery 1981], thus leading to a sooner failure of the coated particle at given conditions. The stress induced in the SiC layer, σ_t, is determined with the following equation valid for a “thin shell” or “soap bubble” pressure vessel of radius r, which is equivalent to the mean radius of the SiC layer, and initial thickness d_o:

$$\sigma_t = \frac{r * p}{2\, d_0} * \left(1 + \dot{v} t / d_0\right) \quad [Pa]$$

The internal gas pressure p is calculated by applying the ideal gas law to the generation of fission gases Xe, Kr, and reaction gas CO. The amount depends on the yield of stable fission gases F_f, burnup Bu, the number of oxygen atoms produced in the kernel O_f, and the temperature T:

$$p = \frac{\left(F_d * F_f + O_f\right) * Bu}{V_f / V_k} * R * T / V_m \quad [Pa]$$

where

F_d is the release fraction of fission gases (Xe, Kr) from the kernel into the void volume;
V_f is the void volume [m^3], typically 50% of the buffer volume;
V_k is the kernel volume [m^3];
V_m is the molar volume of the heavy metal in the kernel [m^3/mole].

Oxygen production in the particle kernels as a result of the fissioning of ^{235}U or ^{239}Pu is strongly dependent on the irradiation history and to a great extent on the type of kernel. Corresponding relationships for O_f were derived from tests at Seibersdorf, Austria, covering an irradiation time up to 550 efpd and a temperature range between 950–1525°C [Proksch 1982]. In case of a transient irradiation temperature history, O_f will be stepwise integrated (upper limit: 0.625). After integration, the total O_f value can be taken to derive, in reverse, a fictitious average irradiation temperature corresponding to that temperature, which would result in the same O_f value, if it were kept constant over the same irradiation time.

The material property “mean SiC strength” and its Weibull distribution as well as their fast fluence dependence are highly significant input parameters. The reference data for SiC strength (836 MPa) and respective Weibull modulus (8.02) for the unirradiated state, typically used in predictive calculations, correspond to a former German coated particle batch production, EO 1607, which represents typical data. It was also the only particle batch, for which SiC strength and Weibull modulus were measured after irradiation in HFR-GM1. In this experiment, the fast fluence achieved was 1.8×10^{25} EDN at an irradiation temperature of 1185°C. The analyzed strength degradation and modulus reduction with fast fluence were 687 MPa and 5.98, respectively. That relationship is usually in PANAMA calculations interpolated or extrapolated to the fast fluences considered, however, with no assured data basis.

The validation of the PANAMA model has been made against numerous experiments with spherical fuel elements heated at accident temperatures in the range of 1600–2500°C. Good agreement with the Kr release measurements was found in many cases. For fuel exposed to extreme irradiation conditions, however, the calculated failure fraction has shown the tendency to overpredict failure.

3.2 Computer Code FRESCO-II

The FZJ computer model FRESCO actually exists in two versions. The “core” version [Krohn 1982] was developed first to describe the fission product release behavior in a pebble-bed core during a core heatup accident phase taking account of redistribution of fission products by the coolant flow and sorption effects at the graphite surfaces of both the fuel elements and the top and bottom reflectors. This FRESCO(-I) version requires the input of transient temperature and coolant flow distribution as the result of a thermodynamic model calculation.

A follow-up version, FRESCO-II [Krohn 1983], concentrates on a single, representative spherical fuel element and includes, in addition to the heating/accident phase, also the phase of irradiation/normal operation. Main purpose of this version was to simulate a complete irradiation and heating experiment for a spherical fuel element. The important input data comprise, apart from the fuel geometry and the temperature–time history, the effective diffusion coefficients for kernel, coating layers, and graphite, as well as a particle failure function given in form of a step function.

The FRESCO diffusion model distinguishes between two types of particles, intact particles and defective/failed particles. From the moment of failure, a particle is treated in the model as a bare kernel which releases activity immediately into the fuel element matrix graphite; the inventory present in the layers at this time is regarded as released. Since the moment

of failure is important, the particles which fail at a certain time are treated in a separate, independent diffusion calculation. For this reason, the number of steps in the failure function is limited to 10. The transport of metallic fission products through the fuel materials is modeled as a transient diffusion process. The transient diffusion equation is typically solved numerically in discrete steps of time and locations with appropriate boundary and interface conditions.

The rate of migration of a species through a homogeneous medium is defined by its mass flux and a concentration gradient as the driving force. According to Fick's first law as described in [Crank 1975], the flux of atoms diffusing through a medium is proportional to the concentration gradient:

$$J_x = -D\frac{\partial c}{\partial x}$$

where
J is the diffusion flux [atoms/(m^2·s)];
D is the diffusion coefficient [m^2/s];
c is the concentration [atoms/m^3];
x is the position or length [m].

The second Fickian law describes the time dependent change of the concentration field by diffusion. Assuming the diffusion coefficient D to be a constant and including source (e.g., production from nuclear fission) and sink (e.g., radioactive decay) terms, Fick's equation, in spherical coordinates, reads as follows:

$$\frac{\partial c}{\partial t} = \nabla\left(D\,\nabla c\right) - \lambda\, c + S$$

where
λ is the decay constant [s^{-1}];
S is the fission product production rate [atoms/(m^3·s)].
and with the boundary conditions that (i) the concentration gradient is 0 at radius r = 0; (ii) continuity of flux and concentration is given at the interface between two adjacent materials; plus a third one describing the mass transfer at the fuel element surface.

The transport velocity of a fission product species in a material is determined by the diffusion coefficient D, m^2/s, which is typically depending on the temperature. For gas-in-gas binary diffusion, the diffusion coefficient is approximately proportional to $T^{1.5}$. For transport in solids, an Arrhenius-type temperature dependence [Jost 1960] of the form

$$D_{eff} = D\left(T,\Gamma,c,...\right) = \sum_{i=1,2} D_{o,i}\,\exp\left\{-\frac{Q_i}{RT}\right\}$$

is assumed where
D_o is the pre-exponential factor [m^2/s];
Q is the activation energy [J/mol];
R is the universal gas constant, = 8.3145 [J/(mol·K)];
T is the absolute temperature [K];

Γ, c is fast neutron fluence and fission product concentration, respectively, as other potential dependencies of D_{eff}.

The transport of mobile fission metals is certainly structure-sensitive and more complex than classical Fickian diffusion and likely a combination of lattice diffusion, grain boundary diffusion, pore diffusion, etc., further complicated by effects like irradiation-enhanced trapping and adsorption. Consequently, any quoted diffusion coefficient should be called an “effective” diffusion coefficient which implies that the overall migration process is approximately described by Fick’s laws [Nabielek 1974].

The procedure of calculation within a time step is performed in two consecutive parts: first the diffusive release from intact and defective particles and from the graphite grains is determined. The sum of those single releases is the overall source term for the fuel element matrix graphite (grain boundaries). In the second part, the diffusive transport through the matrix and release into the coolant is calculated. The diffusion calculation is conducted based on relative values. The inventory of a fission product is built up during the normal operation phase according to its decay constant until reaching 100% at the end of irradiation and beginning of the accident phase, respectively. For long-lived species, the buildup is (almost) linear with irradiation time, while short-lived species quickly reach the equilibrium state.

4 Predictive Calculations for the HFR-EU1 Irradiation Test

4.1 Fuel Performance

Within the IAEA Coordinated Research Program (CRP) on Advances in HTGR Fuel Technologies [IAEA 2012], a benchmark exercise on fuel performance under normal operating conditions has been conducted, in which a prediction of the HFR-EU1 irradiation experiment was one of the examples selected. It was a true prediction, since calculations were made before the test itself had started [Phelip 2006]. Six different fuel performance codes have been applied to this test case assuming operating boundary conditions as were targeted at that time (Table 4).

TABLE 4: Boundary conditions for predictive calculations of fuel performance in HFR-EU1.

	Operating boundary conditions	
	Values as targeted	Values achieved
Irradiation time [efpd]	600	445
Irradiation temperature [°C]	1025 (time/volume averaged)	950 (surface)
Maximum fuel burnup [% FIMA]	20	13.45
Maximum fast neutron fluence [10^{25} n/m^2, E>0.1 MeV]	6.0	4.95
Computer codes involved in benchmark test	ATLAS (France) PANAMA (Germany) COPA (Rep. of Korea) GOLT-V1 (Russia) STRESS3 (UK) PARFUME (USA)	

Results of the fuel performance calculations from all six codes involved are shown in Fig. 7. The results exhibit an excessively broad range: PANAMA predicts the first particle to fail (which is about equivalent to reaching a failure fraction level of 10^{-4}) at a burnup of about 17% FIMA for the irradiation temperature T_{irr} = 1025°C, between 14% FIMA (when assuming T_{irr} = 1100°C) and 20% FIMA (when assuming T_{irr} = 950°C). The Russian GOLT-V1 results, revealing a strong dependence on material properties, show the first particle failure between 14 and 16% FIMA. Calculations with the UK code STRESS3 in connection with the statistical code STAPLE result in a failure fraction exceeding the level of 10^{-4} (or one failed particle) near 14% FIMA. With the US model PARFUME applying two options of calculating CO pressure, two irradiation temperatures, and two sets of SiC strength data, the totally eight predictive calculations for the failure fractions ranges between 4×10^{-8} and 0.43, thus showing tremendous uncertainty margins. The calculation of some 10^7 random particles with the ATLAS code, using a finite element method to calculate the thermal and mechanical performance in connection with a Monte Carlo method, resulted in the assessment of a first particle to fail when the burnup reached approximately 18% FIMA.

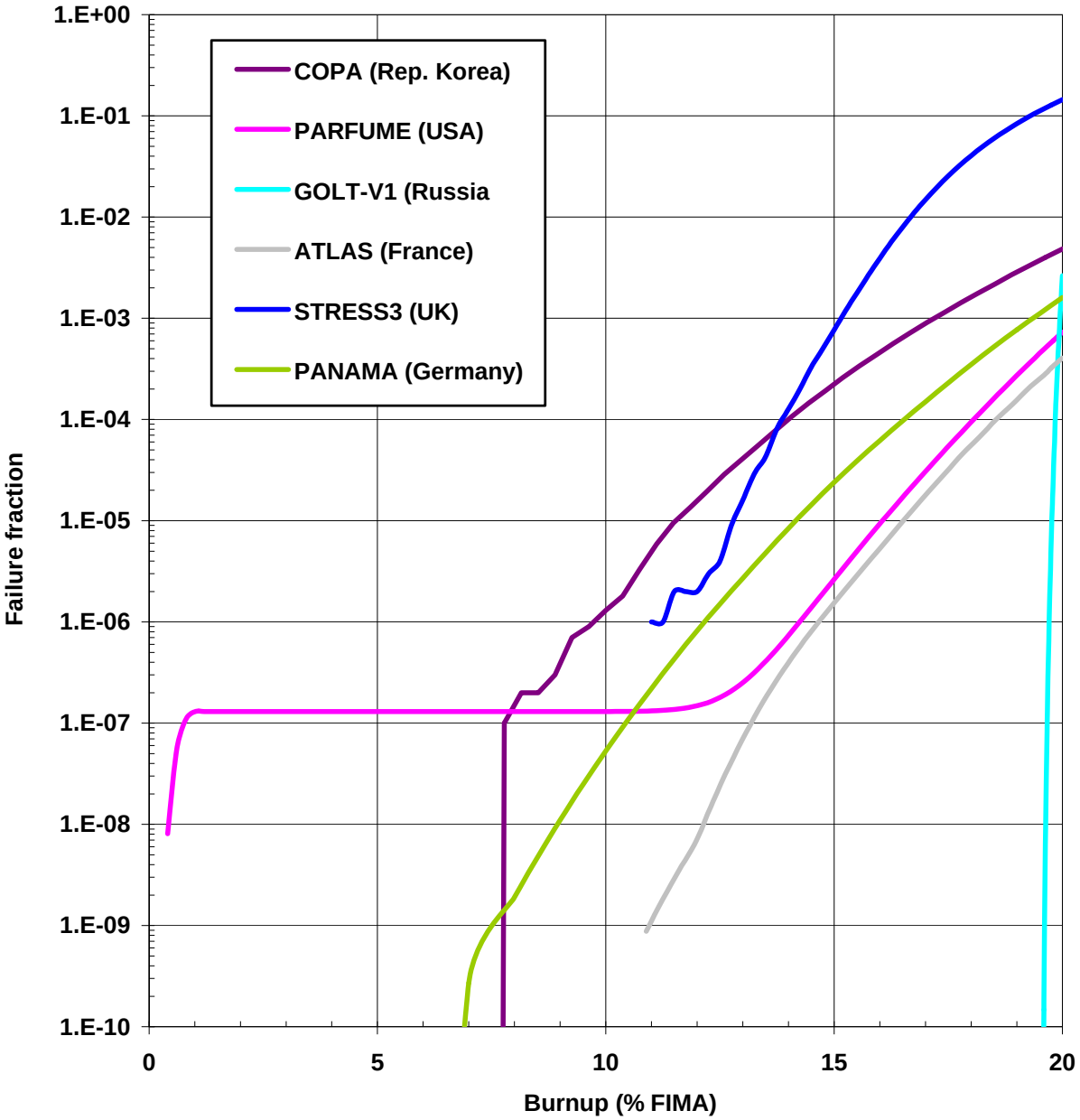

FIGURE 7: Prediction of particle failure probability during the irradiation experiment HFR-EU1 as a function of burnup with various fuel performance codes.

Unfortunately, the target burnups and fast neutron fluences could not be achieved and the achieved burnups and fluences were below those, for which the models predicted first particle failures to occur.

Additional calculation results of the codes are shown in Fig. 8 in terms of total gas pressure (upper figure) and stress induced in the silicon carbide layer (lower figure). Since the calculation of stress distributins in the coating layers is not part of the PANAMA model, no German results are given in the lower figure.

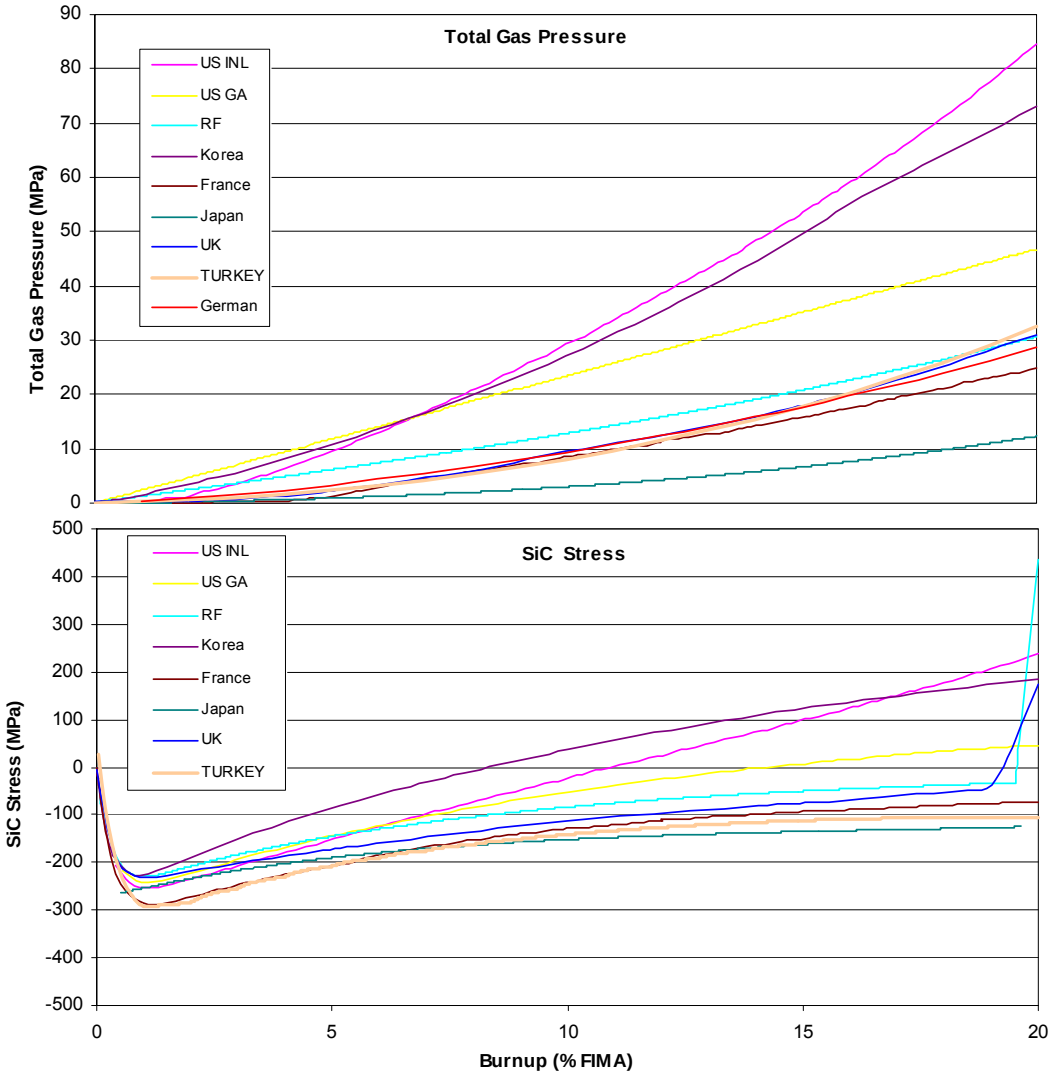

FIGURE 8: Total gas pressure (top) and SiC stresses (bottom) as a function of burnup in the HFR-EU1 irradiation test.

4.2 Metallic Fission Product Release

The objective of another study [Mao 2006], also conducted prior to the irradiation test, was predicting the metallic fission product release behavior during the irradiation test and an assumed postirradiation heating experiment using the FZJ computer codes FRESCO-II and PANAMA. Results for a German (AVR) and a Chinese (INET) fuel sphere during the irradiation phase will be presented in the following.

4.2.1 Assumptions for Test Conditions

Test conditions as were anticipated at that time and on which the predictive calculations were based, are given in Table 5.

TABLE 5. Nominal irradiation characteristics of fuel elements of HFR-EU1 test as originally planned.

	INET spheres		AVR GLE-4 spheres		
Id. No. HFR-EU1/	1	2	3	4	5
Fuel temperature center [°C]	1000	1000	1100	1100	1100
Fuel temperature surface [°C]	890	870	930	930	950
Fission power per FE [kW]	1.45	1.75	2.3	2.15	1.95
Fission power per CP [mW]	171	206	241	225	204
Burnup [% FIMA]	13.7	17.0	21.9	20.8	18.6
Fast neutron fluence [10^{25} n/m^2, E>0.1 MeV]	3.8	4.6	6.0	5.7	5.1

Since FRESCO calculations are conducted for constant temperatures in the fuel sphere, which is not quite correct for the irradiation phase, the code was applied twice selecting both surface and center temperature.

4.2.2 Other Boundary Conditions

By far most of the fissile material is concentrated in the particle kernels surrounded by an intact coating. However, there are small fractions of free uranium present as particle kernels without intact coating and simulated as bare kernels or as contamination of the coating layers and the matrix graphite. The initial U_{free} distribution given in Table 6 is typical for the German reference fuel element and has been used in the calculations. According to the measurements on the HTR-10 first loading fuel, the same above assumptions are also valid for the Chinese fuel spheres.

TABLE 6: Initial distribution of free uranium.

Uranium outside fuel kernel	Inventory fraction U_{free}/U_{tot}
U in buffer	1.0×10^{-3}
U in iPyC	1.0×10^{-4}
U in SiC	1.0×10^{-6}
U in oPyC	1.0×10^{-6}
U in matrix graphite	1.0×10^{-7}

The complement to 100% of the sum of the above fractions is set as the initial kernel inventory. All inventories are assumed to be homogeneously distributed within the respective material zone. The initial distribution of the specific fission product nuclide considered is equivalent to the initial uranium distribution.

The particle failure fractions as input to the FRESCO calculations are represented by a step function with a limited number of steps (≤ 10). Manufacture-induced defective particles typically represent the first step of the failure function. The value representative for the German reference fuel is 3×10^{-5}. For the Chinese spheres, a value of 5×10^{-5} has been taken representative for the average free uranium fraction of the first loading for the HTR-10 [Tang 2001].

Irradiation-induced failure of coated particles may occur during the irradiation. The end-of-life value (EOL) of 2×10^{-5} is the expected value of German reference fuel for the HTR-Modul (10% FIMA) [IAEA, 1997]. For the high burnup fuel elements of the experiment

HFR-EU1, respective PANAMA results were taken, if they exceeded the above German reference value.

The following Table 7 shows the PANAMA results.

TABLE 7: PANAMA results for the irradiation-induced failure fraction of the German and Chinese pebbles in HFR-EU1 at EOL.

HFR-EU1		PANAMA calculation	German reference
German spheres	$T_{irr,sf}$ = 950°C	8.1×10^{-5}	2.0×10^{-5}
(20 % FIMA)	$T_{irr,ce}$ = 1100°C	1.8×10^{-2}	2.0×10^{-5}
Chinese spheres	$T_{irr,sf}$ = 880°C	3.8×10^{-8}	2.0×10^{-5}
(15 % FIMA)	$T_{irr,ce}$ = 1000°C	1.2×10^{-5}	2.0×10^{-5}

As can be seen from the table, the German reference value of 2×10^{-5} is exceeded only for the maximum burnup German spheres in HFR-EU1. In contrast, under the given conditions, the Chinese spheres were predicted to have a lower failure fraction, therefore for conservative reasons, they will be given the same irradiated-induced failure fraction as the German reference.

Table 8 provides the six steps of the failure fraction step functions which were used here for the predictive calculations. Please note that the values for the Chinese spheres start at a higher level due to the higher fraction of free uranium. The step functions are also plotted in Fig. 9.

TABLE 8: Step functions for the particle failure fraction during normal irradiation as input to the FRESCO calculation.

Step No.	Time [efpd]	Particle failure fraction (manufacture-induced plus irradiation-induced)				
		German reference (expected)	German sphere		Chinese sphere	
			950 °C	1100 °C	880 °C	1000 °C
1	0	3.0×10^{-5}	3.0×10^{-5}	3.0×10^{-5}	5.0×10^{-5}	5.0×10^{-5}
2	60	3.4×10^{-5}	3.4×10^{-5}	3.4×10^{-5}	5.4×10^{-5}	5.4×10^{-5}
3	180	3.8×10^{-5}	3.8×10^{-5}	3.8×10^{-5}	5.8×10^{-5}	5.8×10^{-5}
4	300	4.2×10^{-5}	4.2×10^{-5}	4.2×10^{-5}	6.2×10^{-5}	6.2×10^{-5}
5	420	4.6×10^{-5}	4.6×10^{-5}	8.7×10^{-4}	6.6×10^{-5}	6.6×10^{-5}
6	540	5.0×10^{-5}	1.1×10^{-4}	1.8×10^{-2}	7.0×10^{-5}	7.0×10^{-5}

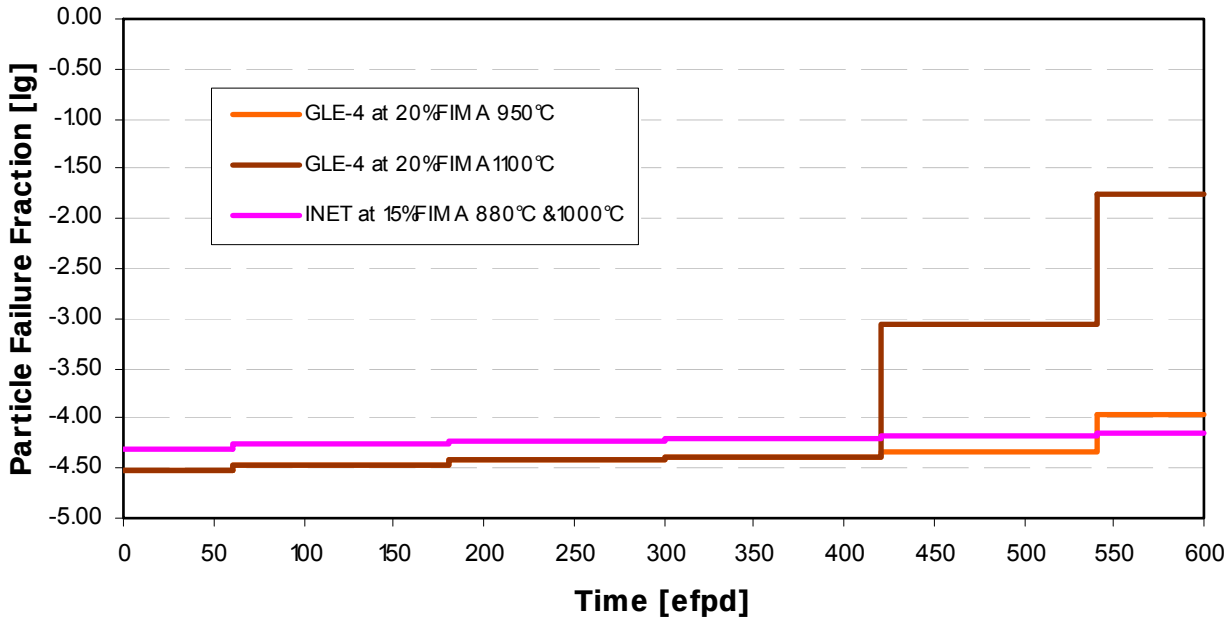

FIGURE 9: Step function for manufacture plus irradiation-induced particle failure as input to the FRESCO predictive calculations of HFR-EU1.

The diffusion coefficients of the different fission product species in the various fuel materials have been chosen according to the recommendations given in [IAEA 1997] for Germany. The sorption effect on graphite surfaces has been neglected in these calculations, rather assuming an unhindered release from the fuel element surface into the coolant.

4.2.3 Radionuclide Release

The calculations of the metallic fission product release with FRESCO were conducted for the isotopes ^{137}Cs, ^{90}Sr and ^{110m} Ag for both the German and the Chinese sphere at final conditions of the HFR-EU1 irradiation test.

Cesium Release

The release behavior of cesium for the AVR fuel element (HFR-EU1/3) is shown in Fig. 10 for the irradiation phase. The blue curves representing the release from the coated particles (@ 950 and 1100°C) are approaching the fraction of failed particles and also following the steps of the failure function towards the end of the irradiation time. This indicates that the cesium release is mainly coming from the failed particles. The two red curves represent the corresponding release from the fuel sphere smoothed by the “buffering” effect of the matrix graphite.

The corresponding cesium release results for the Chinese fuel element (HFR-EU1/1) are given in Fig. 11. The release behavior is similar to the German sphere with the release from the particles closely following the particle failure function. The release from the fuel element remains comparatively low because of the lower temperatures and despite the somewhat higher failure fractions.

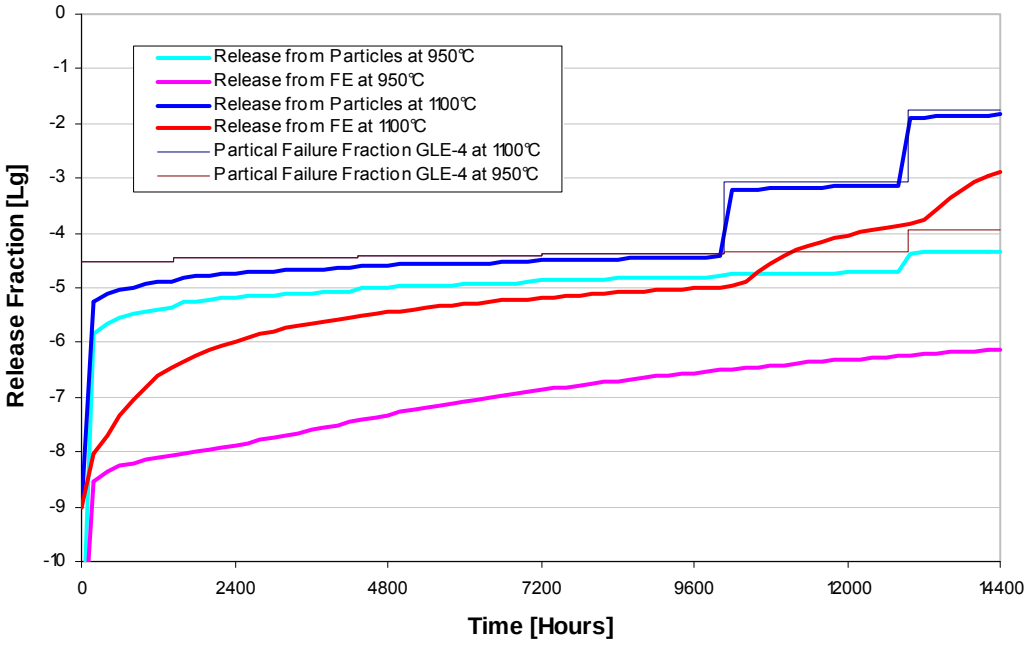

FIGURE 10: Predicted ^{137}Cs release from AVR fuel sphere HFR-EU1/3 during irradiation.

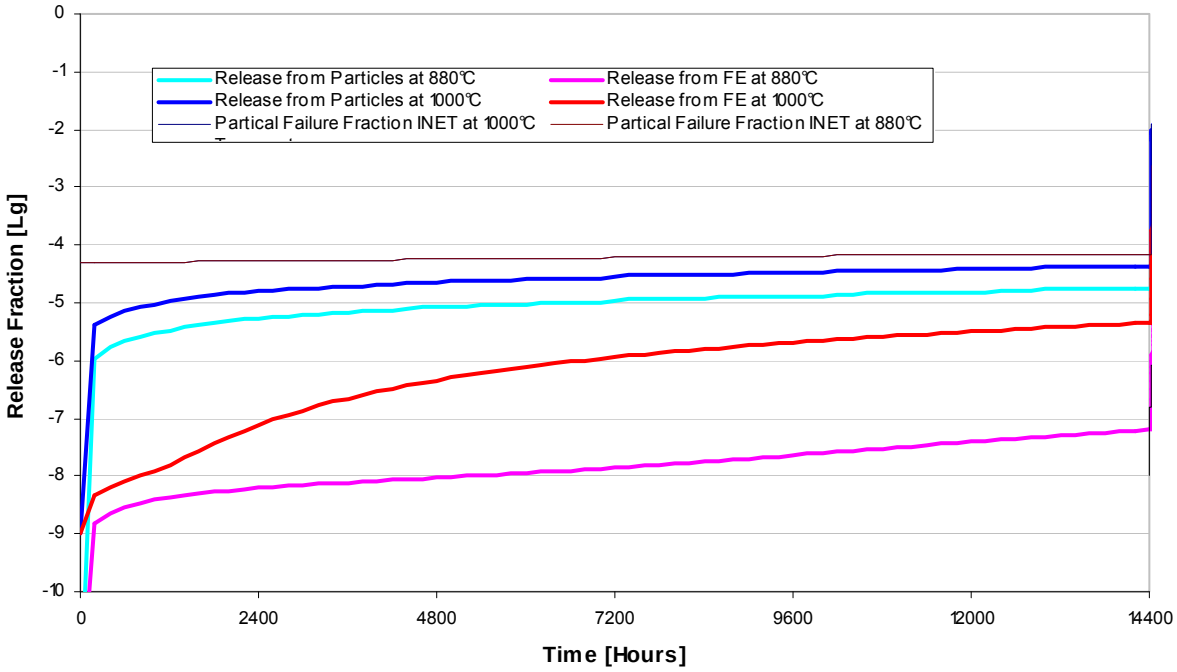

FIGURE 11: Predicted ^{137}Cs release from INET fuel sphere HFR-EU1/1 during irradiation.

Strontium Release

The calculation results for strontium for the cases studied here are shown in Fig. 12 for the AVR sphere and in Fig. 13 for the INET sphere. In general, the strontium release behavior is characterized by a very slow diffusive transport both through the kernel material UO_2 and the matrix graphite. The release from the particle kernels remains very low. This explains why there is no effect on the release curves when there are steps in the failure function.

As can be seen from the plots, the strontium release from the fuel elements remains on a low level during irradiation reaching a value of about 10^{-8}. The difference to the level of release from the particles of three orders of magnitude is due to the slow diffusive transport in the graphite.

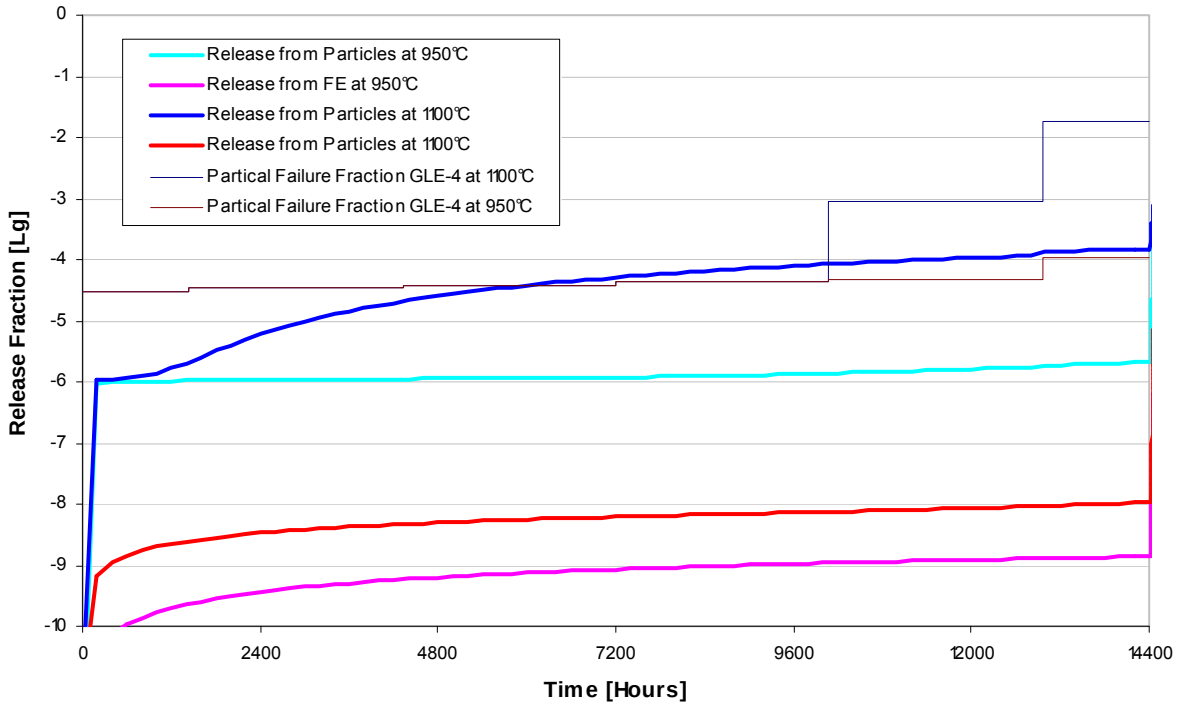

FIGURE 12: Predicted ^{90}Sr release from AVR fuel sphere HFR-EU1/3 during irradiation.

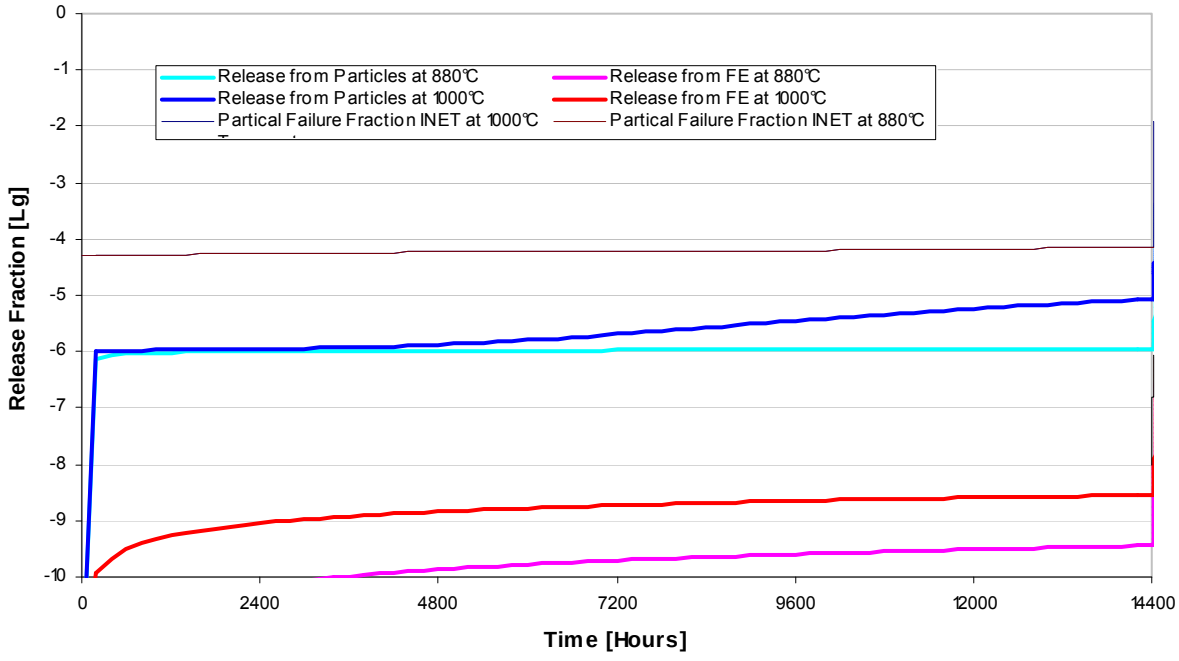

FIGURE 13: Predicted ^{90}Sr release from INET fuel sphere HFR-EU1/1 during irradiation.

Silver Release

The calculated release behavior of ^{110m}Ag is shown in Fig. 14 for the AVR sphere and in Fig. 15 for the INET sphere.

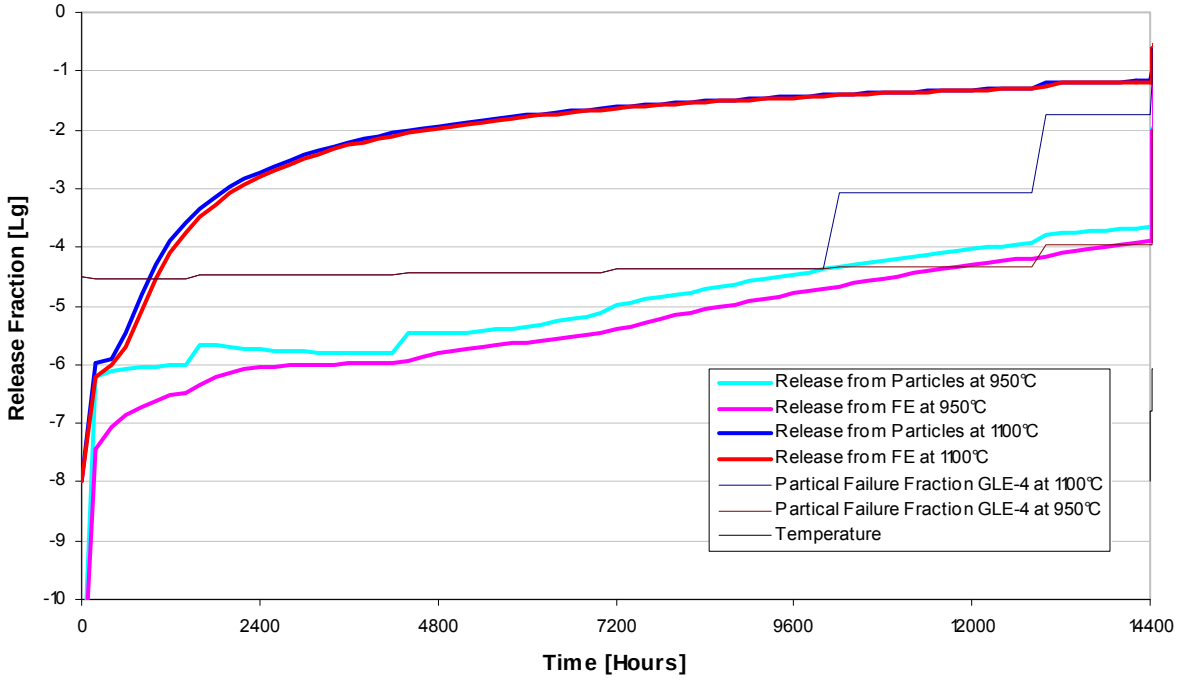

FIGURE 14: Predicted ^{110m}Ag release from AVR fuel sphere HFR-EU1/3 during irradiation.

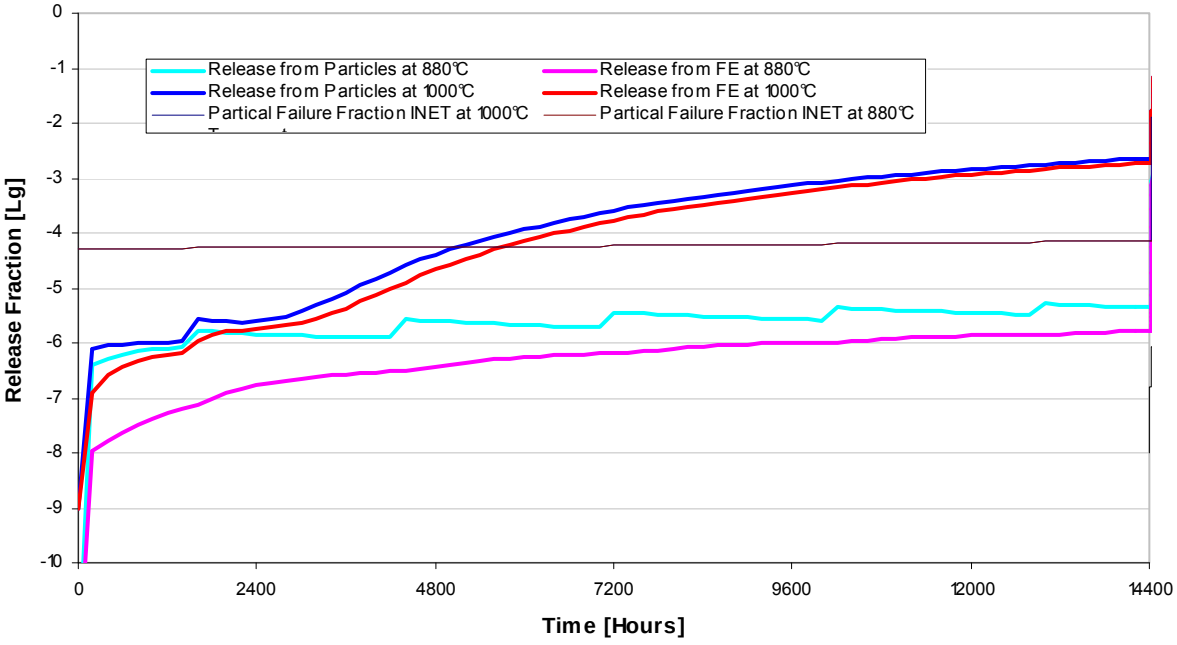

FIGURE 15: Predicted ^{110m}Ag release from INET fuel sphere HFR-EU1/1 during irradiation.

The silver release behavior is typically characterized by a high diffusive transport even through intact coating at temperatures above 1000°C. Furthermore, there is a fast transport of silver through the matrix graphite corresponding to a small retention capability of the graphite. The latter effect can be observed by the fact that in all cases, the curves of Ag release from the particles and from the fuel element are very close or almost identical. The former effect (of a relative rapid transport through intact SiC) can be recognized in the release curves being nearly independent of the particle failure function. Only in the cases of lower temperatures (950°C in Fig. 14 or 880°C in Fig. 15), a step-like release can be identified. The corresponding curves for release from the particles even show partially a decrease in the fractional release (only during irradiation) indicating that at these temperatures, the decay of the silver isotope dominates the diffusive release. Silver release reaches as expected high values already during the irradiation phase which is 0.2% for the Chinese sphere (T_{irr} = 1000°C) and as high as 7% for the German sphere (T_{irr} = 1100°C).

4.2.4 Comparison

In the following Fig. 16, the curves for the fractional release from the fuel element during the HFR-EU1 irradiation phase are plotted again, comparing both the German vs. the Chinese fuel sphere and the three radionuclides considered with silver exhibiting the highest release followed by cesium and then strontium. Table 9 lists the respective EOL data after 600 efpd.

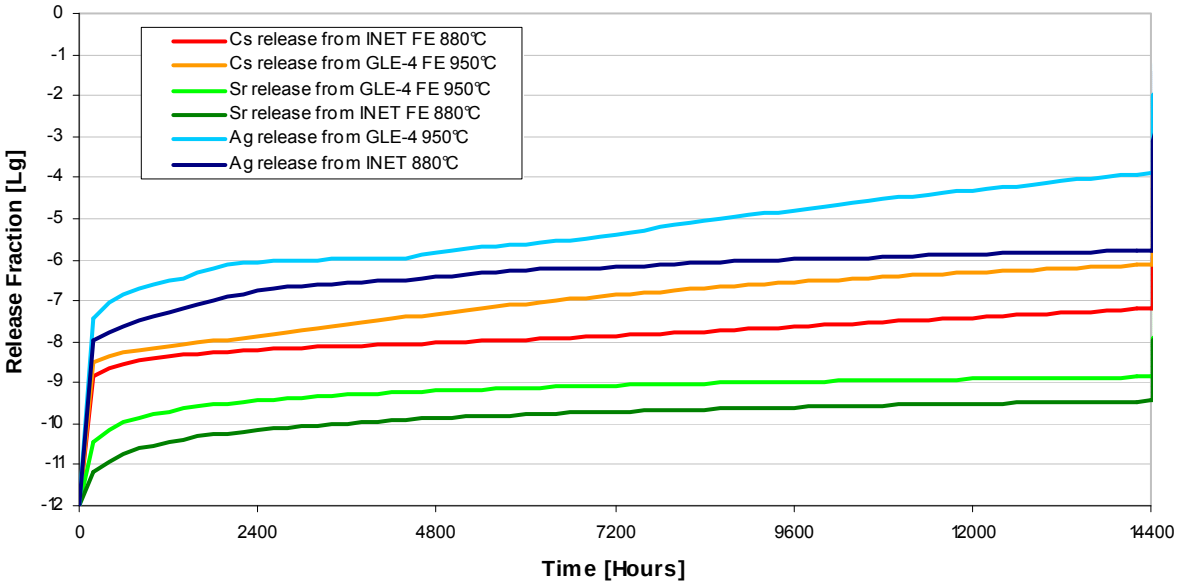

FIGURE 16: Comparison of metallic fission product release during irradiation from the Chinese and German fuel element (irradiation temperature at surface).

Comparing the AVR with the INET fuel element, the curves for the release from the German sphere are, as expected, above those for the Chinese sphere due to the difference in irradiation temperature. Noteworthy is the comparatively small difference in cesium release from the coated particles for surface temperatures between the AVR and INET spheres. Strongest is here given by the fraction of failed particles which is higher in the INET sphere, but the effect being partly compensated by its lower irradiation temperature. In contrast, the differences in the release of silver and strontium are practically due to the temperature difference only.

TABLE 9: Predicted fractional release of ^{137}Cs, ^{90}Sr, and ^{110m}Ag from the German and Chinese fuel spheres at EOL after 600 efpd in the HFR-EU1 experiment.

	Cesium-137 from		Strontium-90 from		Silver-110m from	
	CP	FE	CP	FE	CP	FE
German sphere, burnup 20% FIMA						
T_{irr} = 950°C	4.64×10^{-5}	7.58×10^{-7}	2.12×10^{-6}	1.38×10^{-9}	2.17×10^{-4}	1.28×10^{-4}
T_{irr} = 1100°C	1.45×10^{-2}	1.34×10^{-3}	1.49×10^{-4}	1.08×10^{-8}	6.73×10^{-2}	6.61×10^{-2}
Chinese sphere, burnup 15% FIMA						
T_{irr} = 800°C	1.77×10^{-5}	6.37×10^{-8}	1.11×10^{-6}	3.59×10^{-10}	4.40×10^{-6}	1.70×10^{-6}
T_{irr} = 1000°C	4.28×10^{-5}	4.44×10^{-6}	8.67×10^{-6}	2.84×10^{-9}	2.29×10^{-3}	1.92×10^{-3}

For the specified operating conditions of the reactor design considered and for the typical German reference spherical fuel element, the results show that under the given thermal hydraulic boundary conditions, the release remains on a very low level for all radionuclides investigated. For cesium, the dominant release is from defective/failed particles. The release of strontium remains always insignificant due to its enormous retention capability in matrix and kernel material. Silver release is low during normal operation similar to cesium, but shows significant release, even from intact coated particles under the conditions of elevated temperatures above 1000°C.

5 Postcalculation of the HFR-EU1 Irradiation Test

Calculations habe been made for an AVR sphere (HFR-EU1/3) and an INET sphere (HFR-EU1/1).

5.1 Fuel Performance

5.1.1 Boundary Conditions

In the HFR-EU1 irradiation experiment, a total of 34 thermocouples were installed to measure temperatures at or near the surfaces of the five fuel spheres. During the course of irradiation, unfortunately, many thermocouples failed. It was particularly for the AVR spheres at positions with the higher impact of temperature and fast neutron fluxes that, at some point, all thermocouples at the sphere positions failed such that no temperature measurements became available (see also Table 3).

Table 10 lists the averaged temperatures for the five fuel spheres during each of the 16 irradiation cycles (see also Fig. 2). Question marks indicate positions and times with no temperature measurements. For the calculations, the last measured temperature was assumed constant for the remaining irradiation time.

TABLE 10: Temperatures of the five HFR-EU1 spheres during the irradiation cycles.

Cycle	Accumulated irradiation time [efpd]	Temperature in HFR-EU1 [°C]				
		Sphere 1	Sphere 2	Sphere 3	Sphere 4	Sphere 5
		(INET)			(AVR)	
06-08	24.2	800	901	946	969	965
06-09	51.1	832	923	926	949	938
06-10	79.7	820	929	939	953	931
07-01	107.5	852	941	929	946	930
07-02	136.4	840	933	951	957	956
07-03	164.3	821	939	930	945	951
07-07	191.2	828	933	933	936	926
07-08	220.4	810	948	936	949	942
07-09	248.4	831	924	948	941	934
07-10	276.2	819	944	?	941	981
08-01	304.0	839	926	?	949	?
08-02	332.8	849	943	?	936	?
09-08	357.6	810	901	?	?	?
09-09	389.0	864	943	?	?	?
09-10	413.2	833	931	?	?	?
10-01	444.9	873	943	?	?	?

Tables 11 and 12 contain the estimated fast neutron fluences and the pre-calculated burnups [Laurie 2010a]. Burnup development with time for all fuel spheres was also shown already in Fig. 3.

To allow for a more detailed fuel performance assessment, each irradiation cycle is subdivided into two halfs, which makes it a total of 32 PANAMA calculations for each sphere.

TABLE 11: Preliminary fast neutron fluence of the HFR-EU1 spheres during the irradiation cycles.

Cycle	Accumulated irradiation time [efpd]	Fast neutron fluence evolution in HFR-EU1 [10^{25} n/m^2, E>0.1 MeV]				
		Sphere 1	Sphere 2	Sphere 3	Sphere 4	Sphere 5
		(INET)			(AVR)	
06-08	12.1	0.056		0.088		
06-08	24.2	0.099		0.156		
06-09	37.65	0.155		0.244		
06-09	51.1	0.210		0.332		
06-10	65.4	0.305		0.481		
06-10	79.7	0.399		0.630		
07-01	93.6	0.494		0.780		
07-01	107.5	0.588		0.929		
07-02	121.95	0.691		1.091		
07-02	136.4	0.793		1.252		
07-03	150.35	0.890		1.406		
07-03	164.3	0.988		1.560		
07-07	178.00	1.093		1.726		
07-07	191.2	1.158		1.829		
07-08	206.05	1.310		2.069		
07-08	220.4	1.422		2.246		
07-09	234.4	1.531		2.418		
07-09	248.4	1.640		2.589		
07-10	262.3	1.744		2.754		
07-10	276.2	1.848		2.918		
08-01	290.1	1.951		3.080		
08-01	304.0	2.053		3.241		
08-02	318.4	2.165		3.419		
08-02	332.8	2.278		3.597		
09-08	345.2	2.373		3.747		
09-08	357.6	2.468		3.897		
09-09	373.3	2.590		4.089		
09-09	389.0	2.711		4.281		
09-10	401.1	2.804		4.427		
09-10	413.2	2.896		4.573		
10-01	429.05	3.016		4.762		
10-01	444.9	3.135		4.950		

Fast neutron fluence (maximum → sphere 3) from Table in [Laurie 2010a]
Ratio of final fluence of sphere 1 to that of sphere 3 to yield transient fluence data for sphere 1

TABLE 12: Preliminary burnups of the HFR-EU1 spheres during the irradiation cycles.

Cycle	Accumulated irradiation time [efpd]	Burnup evolution in HFR-EU1 [% FIMA]				
		Sphere 1	Sphere 2	Sphere 3	Sphere 4	Sphere 5
		(INET)			(AVR)	
06-08	12.1	0.227	0.288	0.382	0.388	0.357
06-08	24.2	0.454	0.576	0.764	0.775	0.714
06-09	37.65	0.700	0.888	1.174	1.193	1.102
06-09	51.1	0.945	1.199	1.583	1.610	1.490
06-10	65.4	1.199	1.524	2.001	2.034	1.889
06-10	79.7	1.453	1.849	2.419	2.458	2.287
07-01	93.6	1.717	2.190	2.845	2.897	2.683
07-01	107.5	1.980	2.531	3.270	3.335	3.079
07-02	121.95	2.254	2.881	3.703	3.784	3.487
07-02	136.4	2.527	3.231	4.136	4.232	3.895
07-03	150.35	2.781	3.559	4.539	4.650	4.273
07-03	164.3	3.034	3.886	4.941	5.067	4.650
07-07	178.00	3.371	4.320	5.472	5.618	5.166
07-07	191.2	3.708	4.753	6.002	6.168	5.681
07-08	206.05	4.067	5.223	6.562	6.749	6.226
07-08	220.4	4.425	5.692	7.122	7.330	6.771
07-09	234.4	4.764	6.124	7.634	7.861	7.272
07-09	248.4	5.102	6.555	8.146	8.391	7.773
07-10	262.3	5.437	6.964	8.626	8.887	8.245
07-10	276.2	5.753	7.372	9.105	9.383	8.716
08-01	290.1	6.068	7.762	9.557	9.850	9.161
08-01	304.0	6.382	8.151	10.008	10.316	9.605
08-02	318.4	6.697	8.538	10.449	10.772	10.041
08-02	332.8	7.012	8.924	10.890	11.227	10.476
09-08	345.2	7.276	9.245	11.251	11.599	10.833
09-08	357.6	7.539	9.565	11.612	11.971	11.190
09-09	373.3	7.863	9.955	12.045	12.417	11,619
09-09	389.0	8.186	10.344	12.477	12.863	12.048
09-10	401.1	8.429	10.634	12.796	13.191	12.365
09-10	413.2	8.672	10.924	13.114	13.518	12.681
10-01	429.05	8.979	11.286	13.509	13.923	13.073
10-01	444.9	9.285	11.648	13.903	14.328	13.465

The above given boundary conditions of burnup, and fast neutron fluence for the two considered fuel spheres are shown in Fig. 17 as a function of irradiation time.

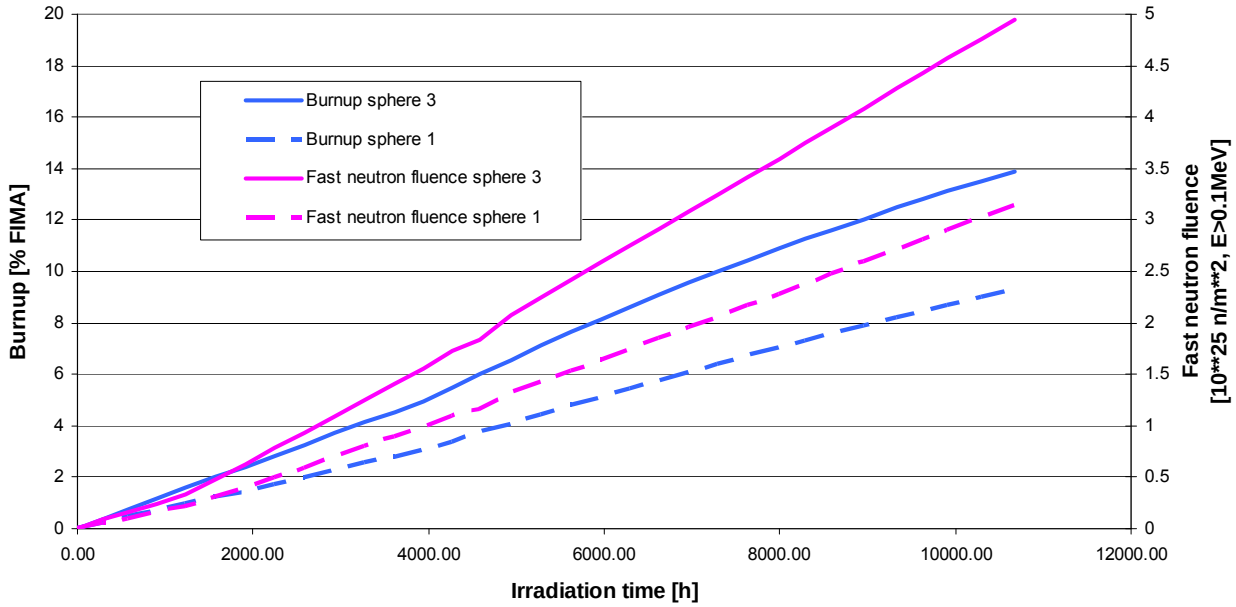

FIGURE 17: Estimated burnup (blue) and fast neutron fluence (red) of sphere 3 (AVR) (solid curves) and sphere 1 (INET) (dashed curves) during the irradiation experiment HFR-EU1.

The median silicon carbide strength and the Weibull modulus characterizing the Weibull distribution of the strength, both essential input parameters to the PANAMA fuel performance model, are decreasing with fast fluence. Respective curves for the two considered fuel spheres are given in Fig. 18 as a function of irradiation time.

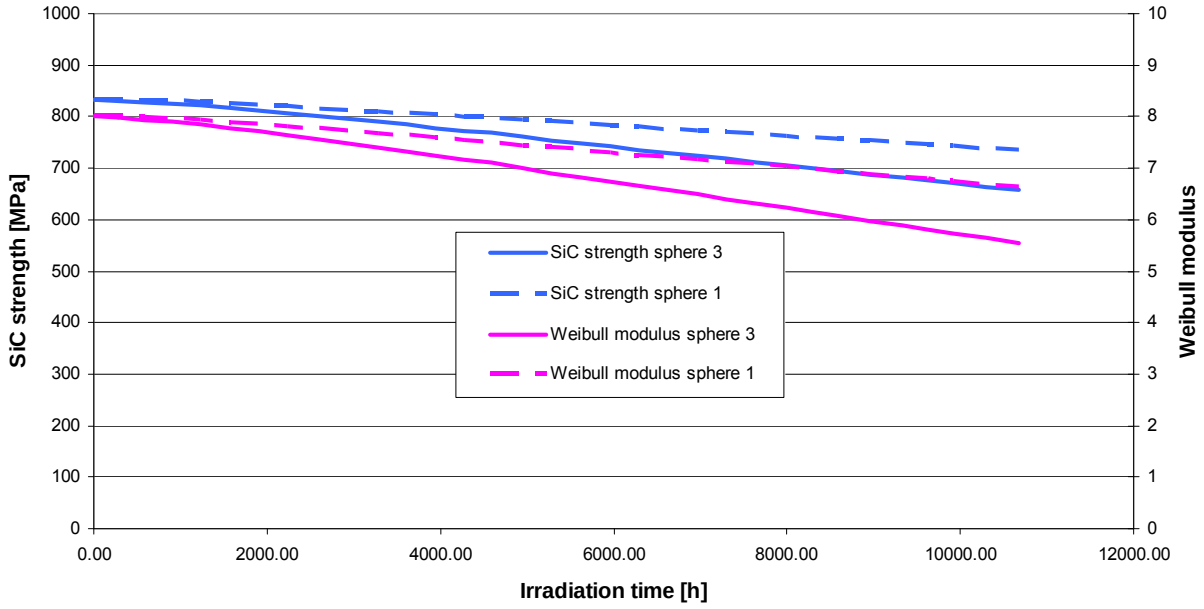

FIGURE 18: Decrease of the median SiC strength (blue) and Weibull modulus (red) with fast neutron fluence for sphere 3 (AVR) (solid curves) and sphere 1 (INET) (dashed curves) during the irradiation experiment HFR-EU1.

5.1.2 Results

The results of the PANAMA calculations for sphere 3 (AVR) and sphere 1 (INET) are shown in the following two figures. Figure 19 provides the development of total gas pressure inside the TRISO particles with irradiation time, which leads as expected to higher pressures in the AVR particles. The contribution to the pressure by CO gas generation indicated by the red curves is negligible.

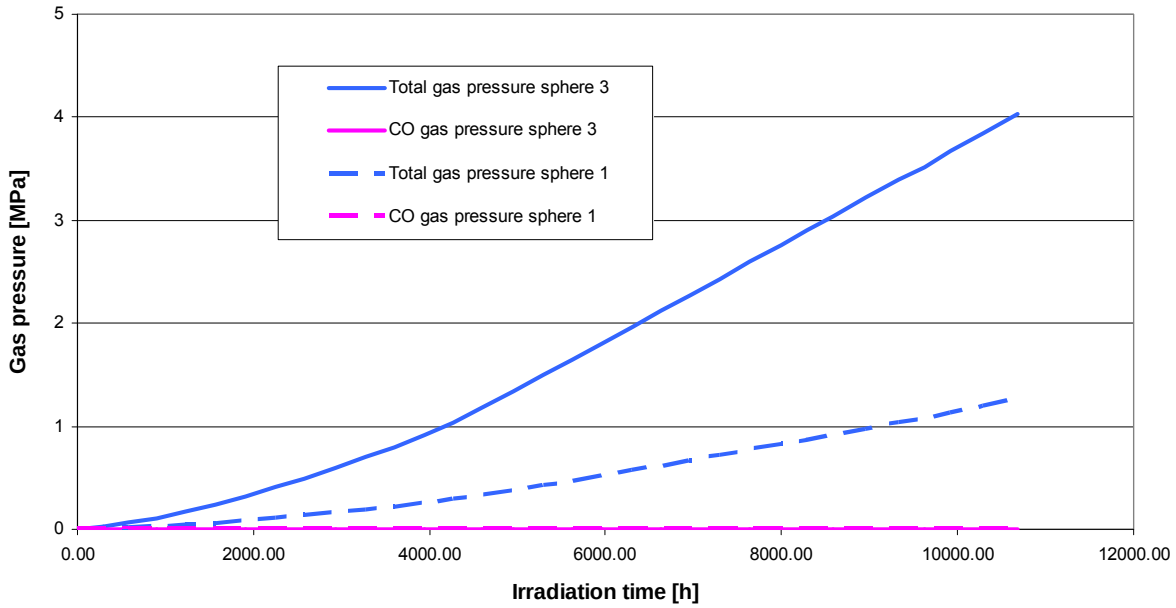

FIGURE 19: Development of total gas pressure (blue) and CO gas pressure (red) with irradiation time during the irradiation experiment HFR-EU1.

In Fig. 20, the failure probabilities of the TRISO particles in the AVR sphere (solid curves) and INET sphere (dashed curves) are displayed. The blue curves refer to the irradiation phase where no particle failure is expected to occur for the Chinese sphere, while for the AVR sphere, failure fraction is approaching the level of one failed particle towards the end of the test.

The red curves indicate the failure fraction predicted to occur after a subsequent 200 hours heating phase at 1600°C as a function of the irradiation state of the coated particles. For the Chinese sphere, the dashed curve shows that one particle may fail after the additional heating phase, while it is in the order of 1000 particles (~10%) for the AVR sphere.

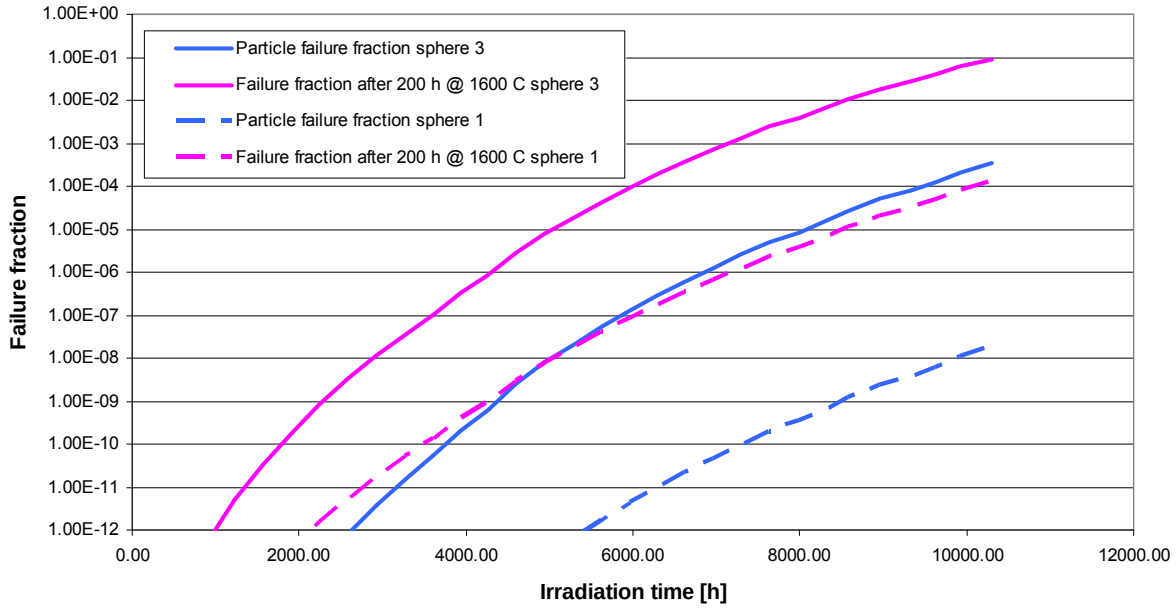

FIGURE 20: Particle failure probability during the irradiation experiment HFR-EU1 (blue) and after a 200-h 1600°C heating phase as a function of irradiation time.

5.2 Metallic Fission Product Release

Based on the temperature input as given in Table 10, the FRESCO-II code has been applied to calculate the metallic fission product release behavior during the irradiation test.

5.2.1 Assumptions for Test Conditions

According to the observation of very low fission gas release levels throughout the irradiation test, the particle failure fraction was assumed zero in the calculations. Other boundary conditions such as the initial distribution of free uranium or the diffusion coefficients assumed were kept the same as in the predictive study described in chapter 4.

Since FRESCO calculations are conducted for constant temperatures in the fuel sphere, which is not quite correct for the irradiation phase, the code was applied twice selecting both surface and center temperature. Since the (measured) surface temperature is still unknown, center temperatures of 1100°C (AVR) and 1000°C (INET), respectively, were taken.

5.2.2 Radionuclide Release

The calculations of the metallic fission product release with the diffusion code FRESCO have been conducted for the radiologically relevant isotopes ^{137}Cs, ^{90}Sr and ^{110m}Ag.

The release behavior for the AVR fuel element during irradiation for all three isotopes is shown in Fig. 21 for the surface temperature measured and in Fig. 22 for the center temperature (of 1100°C) assumed.

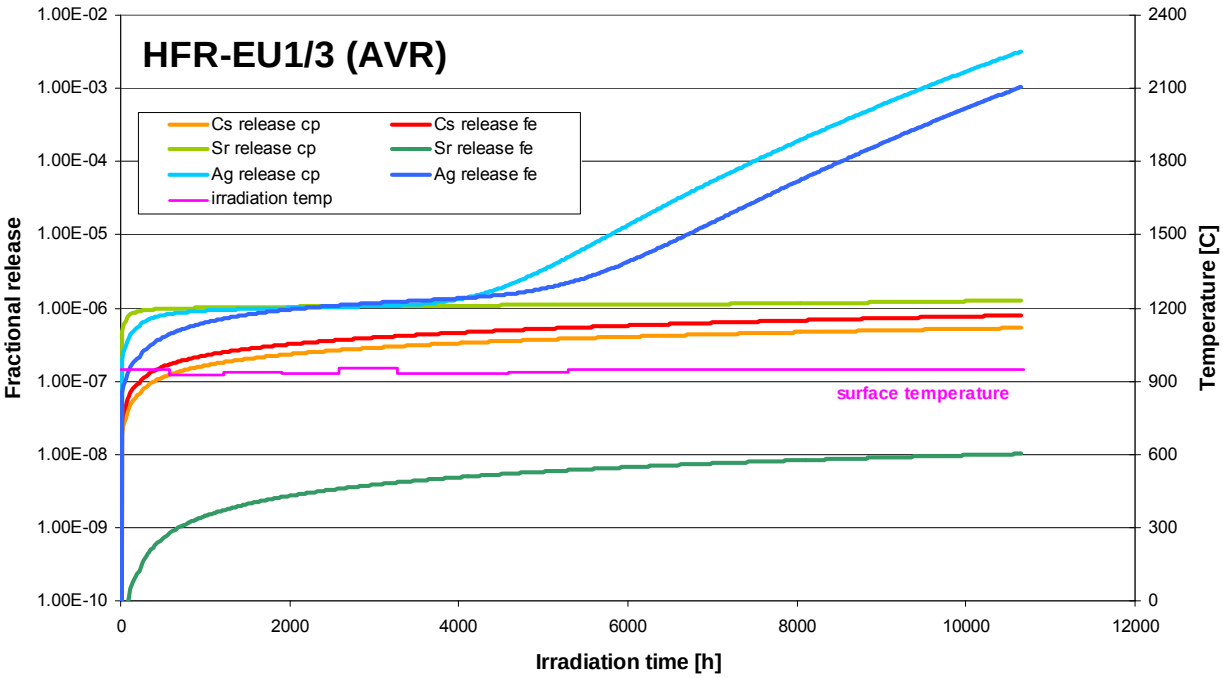

FIGURE 21: Calculated metallic fission product release from fuel sphere HFR-EU1/3 (AVR) during irradiation (surface temperature) based on achieved irradiation data.

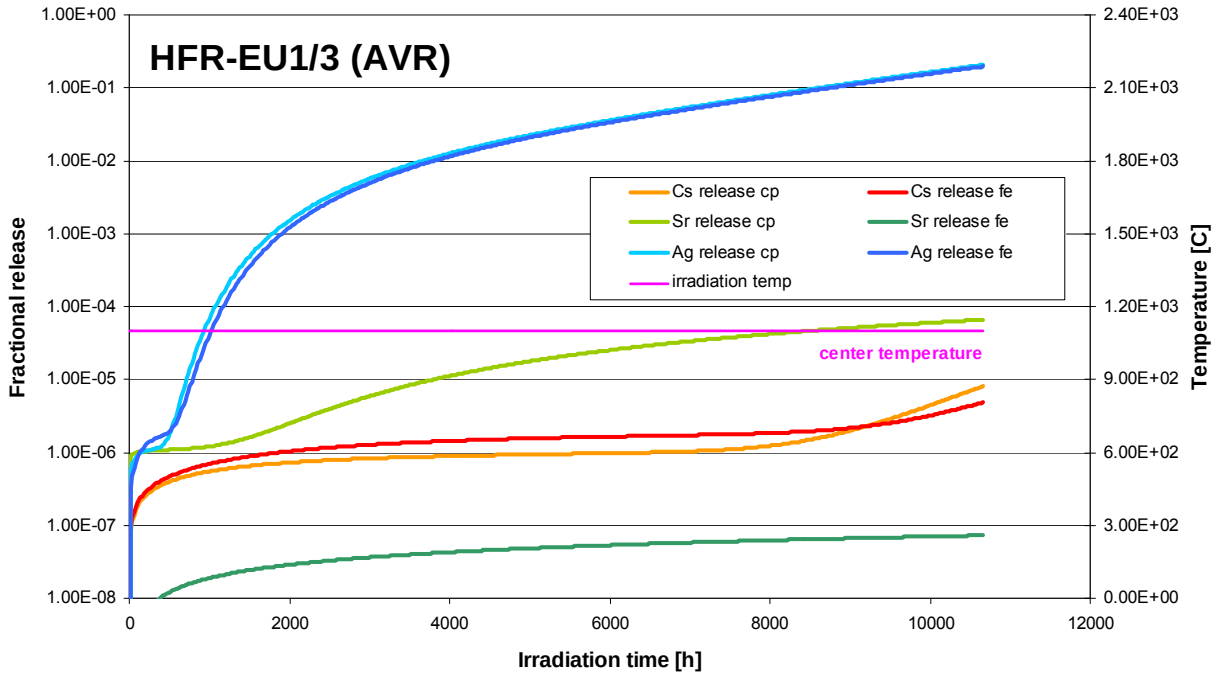

FIGURE 22: Calculated metallic fission product release from fuel sphere HFR-EU1/3 (AVR) during irradiation (center temperature) based on achieved irradiation data.

Cesium release (reddish curves) from the coated particles (orange) and from the fuel element (red) remain below the level of 10^{-6} (surface temperature) and, for the center temperature, approach 10^{-5} towards the end of the test, still below the level of the inventory of a coated particle.

Strontium release (greenish curves) from the coated particles (light green) is somewhat higher compared to cesium, but is completely retained in the fuel element, the release from which remains even for the higher temperature below 10^{-7}. The difference to the level of release from the particles of three orders of magnitude is due to the slow diffusive transport in the graphite.

In contrast and as expected, silver release (blue curves), which is typically characterized by a high diffusive transport even through intact coating at temperatures above 1000°C, rises rapidly reaching final release fractions of 0.1% (surface) and 20% (center), respectively. Furthermore, there is a fast transport of silver through the matrix graphite corresponding to a small retention capability of the graphite. The latter effect can be observed by the fact that in all cases, the curves of Ag release from the particles and from the fuel element are very close or almost identical.

The corresponding fractional release curves for the Chinese fuel element are shown in Fig. 23 based on the measured surface temperature, and in Fig. 24 based on the assumed center temperature of 1000°C.

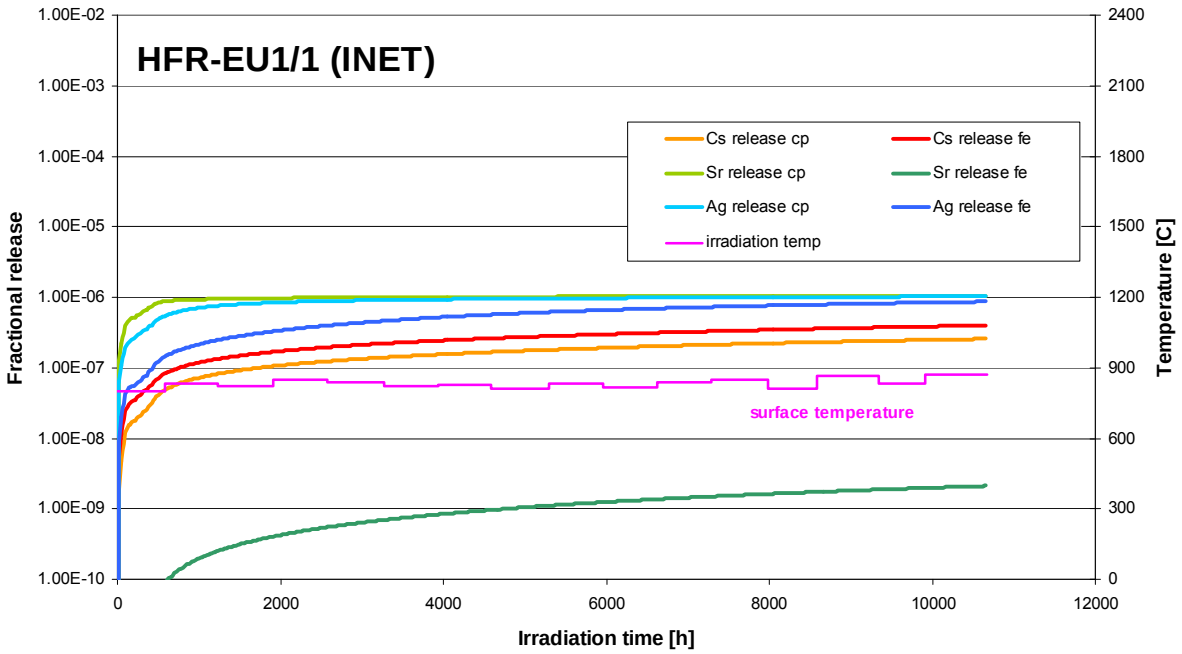

FIGURE 23: Calculated metallic fission product release from fuel sphere HFR-EU1/1 (INET) during irradiation (surface temperature) based on achieved irradiation data.

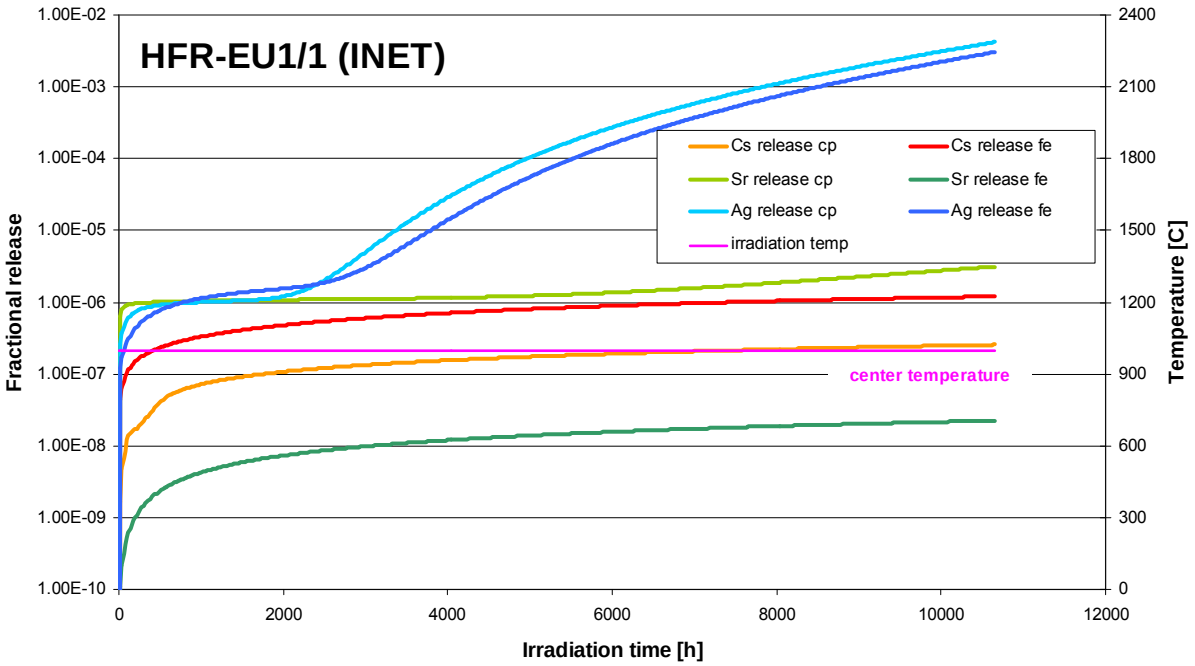

FIGURE 24: Calculated metallic fission product release from fuel sphere HFR-EU1/1 (INET) during irradiation (center temperature) based on achieved irradiation data.

The results are qualitatively similar to those for the AVR sphere except being on a lower level due to the 100°C lower irradiation temperature. Final fractional release data calculated are 1.2×10^{-6} for cesium, 2.3×10^{-8} for strontium, and 3.1×10^{-3} for silver.

5.2.3 Variation

Statistical Distribution of Kernel Diameter and Layer Thicknesses

Mechanical performance modeling of coated particles is based on the concept that the pressure in the buffer layer induces stresses in the coating layers and when these stresses exceed the strength, the coating fails. However, this is the situation that describes the expected 50% failure level. In modern, high performing fuel, the interest is more at the 10^{-5} failure fraction level and this requires the consideration of statistical variations in material properties and geometrical data. In the modern TRISO particle, the silicon carbide layer defines the strength of the coating and the primary statistics under consideration is the Weibull distribution of SiC strengths. Higher pressure occurs with small buffer thicknesses due to the smaller volume, and with larger fuel kernels due to the higher fission product inventory.

Using the data for typical UO_2 LTI TRISO particle geometrical data for the example of HFR-EU1/ AVR Reload 21-2 data, the predicted frequency distribution of gas pressures in 1,000,000 particles is shown in Fig. 25. The statistical variations assumed were 502.2 ± 10.6 µm for the kernel diameter, and 94.3 ± 13.0 µm for the buffer thickness. The variation of pressures ranges between 24 MPa and 82 MPa after 1100°C irradiation to 20% FIMA occurring in particles with different kernel diameters and buffer thicknesses. The gas pressure under nominal conditions is 44 MPa.

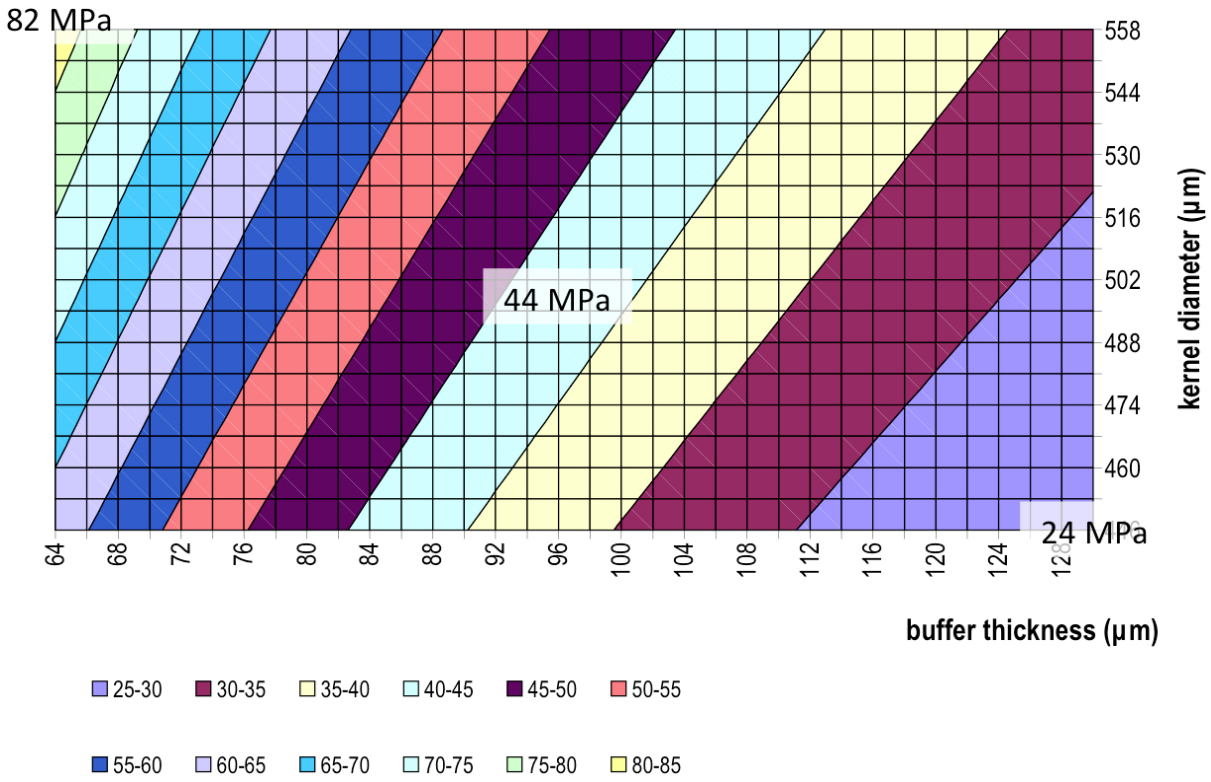

FIGURE 25: Pressure variation after 1100°C irradiation to 20% FIMA in particles with different kernel diameters and buffer thicknesses.

The corresponding results for the mechanical coating failure fractions are shown in Fig. 26. Predictions for failure fractions are increasing with the statistical approach, but are not significantly larger than those from the classical approach. This increases the failure prediction, the difference is however marginal.

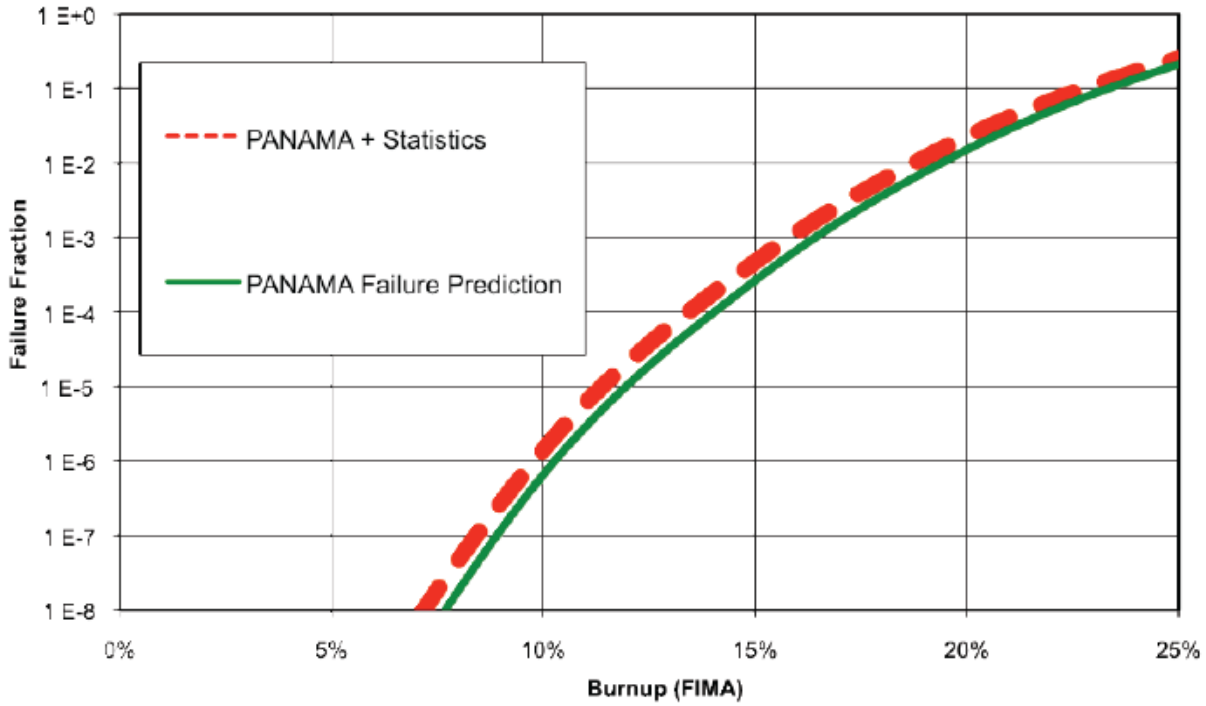

FIGURE 26: Prediction of mechanical coating failure with/without statistics of kernel diameter and buffer thickness.

Many modern TRISO particle performance codes use Monte-Carlo sampling (STAPLE, ATLAS, PARFUME, and others) and this is ultimately equivalent. The problem is that to get a 10^{-6} failure prediction with 1% certainty, it is necessary to take 10^{8} samples and this might be time-consuming. Doing the convolution with integration over all possibilities is just simpler and more precise.

When allowing statistical distributions in buffer and SiC thickness, the predicted particle failure fractions for a given range of buffer layer thicknesses and SiC layer thicknesses particles may vary between ~10^{-9} and ~10^{-3}. Failure fraction with reference dimensions is predicted at 6.8×10^{-7}.

Assuming in the statistical approach a variation in buffer thickness of 95.0 ± 13.0 µm and in SiC layer thickness of 35.0 ± 2.0 µm, and a temperature of 1100°C, coating failure is predicted as shown in Fig. 27.

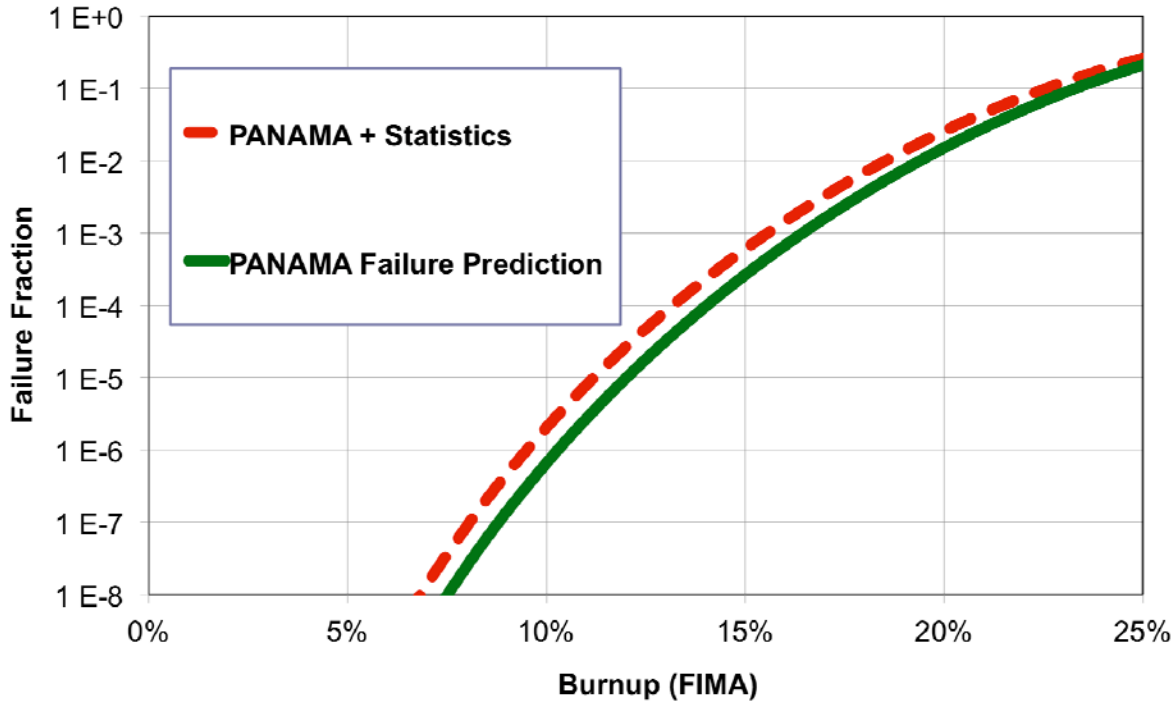

FIGURE 27: Prediction of mechanical coating failure with/without statistics of buffer thickness and SiC thickness.

6 Conclusions

Within the frame of the ARCHER project, R&D activities have been starting to evaluate the irradiation experiment HFR-EU1. The study presented here is dealing with the calculations of fuel performance and metallic fission product release during irradiation based on the operational data available up to now, and also includes a comparison with predictive calculations from the past. The results can be summarized as follows:

- Prediction of fuel performance conducted within the IAEA CRP-6 expects a first coated particle to fail at ~17% FIMA burnup. The recent calculation would see an earlier first particle failure at ~13% FIMA. Reason is the higher irradiation temperature assumed, but a thorough evaluation of the EU1 sphere temperature is still pending. Calculating one single event towards the end of the test is not in disagreement with the observation that no coated particle (pressure-vessel-) failed during irradiation.

- With regard to metallic fission product release during irradiation, silver release is expected to be highest with an EOL fractional release in the percentage range. In contrast, release of cesium and strontium from the fuel spheres will remain at a low level. Since respective experimental data are not available yet, the new calculations still have predictive character.

- Only in case of SiC layer failure with the outer pyrocarbon layer remaining intact (as obviously occurred in the high-temperature irradiation experiment HFR-EU1bis), cesium release might go up to higher values.

- The consideration of the statistical variation of kernel diameters and layer thicknesses allows a look at the extreme ends of the manufacturing processes. Integral results reveal a somewhat higher particle failure fraction in the statistics approach compared to the use of nominal data. But considering the uncertainties in material property data, the difference is small and the model predictions with nominal dimensions are judged to be satisfactory.

On-going PIE done at the HFR in Petten and the ITU in Karlsruhe will provide more detailed insight into the irradiation behavior of the EU1 fuel spheres.

7 References

Bongartz, K., Gyarmati, E., Schuster, H., Täuber, K., The brittle ring test: A method for measuring strength and Young's modulus on coatings of HTR fuel particles. *Journal of Nuclear Materials* **62** (1976) 123.

Crank, J., The mathematics of diffusion. 2nd Edition., Oxford University Press, New York (1975).

Fütterer, M.A:, et al., Results of AVR fuel pebble irradiation at increased temperature and burn-up in the HFR Petten. *Nuclear Engineering and Design* **238** (2008) 2877.

Groot, S. de, et al., The European ARCHER project proposal: HTR research towards demonstration. Proc. 5th Int. Top. Meeting on High Temperature Reactor Technology HTR2010, Prague (2010).

IAEA, Fuel Performance and Fission Product Behavior in Gas Cooled Reactors. Report IAEA-TECDOC-978, International Atomic Energy Agency, Vienna (1997).

IAEA, Advances in HTGR fuel technology. Report IAEA-TECDOC-1674, International Atomic Energy Agency, Vienna (2012).

Jost, W., Diffusion in solids, liquids, gases. 3rd Printing with Addendum, Academic Press, New York (1960).

Krohn, H., Freisetzung von Spaltprodukten aus dem Core eines Kugelhaufenreaktors bei Störfällen mit Core-Aufheizung. Report Jül-1791, Research Center Jülich (1982).

Krohn, H., Finken, R., FRESCO-II: Ein Rechenprogramm zur Berechnung der Spaltproduktfreisetzung aus kugelförmigen HTR-Brennelementen in Bestrahlungs- und Ausheizexperimenten. Report Jül-Spez-212, Research Center Jülich (1983).

Laurie, M., et al., Results of the HFR-EU1 fuel irradiation of INET and AVR pebbles in the HFR Petten. Proc. 5th Int. Top. Meeting on High Temperature Reactor Technology HTR2010, Prague (2010a).

Laurie, M., et al., JRC's on-line fission gas release monitoring system in the High Flux Reactor Petten. Proc. 5th Int. Top. Meeting on High Temperature Reactor Technology HTR2010, Prague (2010b).

Mao, Y., Prediction of Metallic Fission Product Release Behaviour in Spherical Fuel Elements Irradiated in the Experiment HFR-EU1 during Normal Irradiation and under Heating Conditions. Studienarbeit at the Fachhochschule Jülich (2006).

Marmier, A., Fütterer, M.A., Laurie, M., Tang, C.H., Preliminary results of the HFR-EU1 fuel irradiation of INET and AVR pebbles in the HFR Petten. Proc. 4th Int. Top. Meeting on High Temperature Reactor Technology HTR2008, Washington, DC (2008).

Montgomery, F.C., Fission product – SiC reaction in HTGR fuel. Report GA-905837/1, General Atomics, San Diego, CA (1981).

Nabielek, H., et al., Performance limits of coated particle fuel; Part III: Fission product mgration in HTR fuel. Report D.P.828, Part 3, Dragon Project, Winfrith (1974).

Phelip, M., et al., The CRP-6 benchmark on HTGR fuel behavior under normal operation. Int. Congress on Advances in Nuclear Power Plants ICAPP'06, Reno (2006).

Proksch, E., et al., Production of carbon monoxide during burnup of UO_2 kerneled HTR fuel particles. *Journal of Nuclear Materials* **107** (1982) 280.

Tang C.H., et.al., Fabrication of the first loading fuel of 10 MW high temperature gas-cooled reactor. HTR-TN Int. HTR Fuel Seminar, Brussels (2001).

Van der Merwe, H., Olivier, D., Modeling silver: Evaluation of German experience. Proc. 4th Int. Top. Meeting on High Temperature Reactor Technology HTR2008, Washington, DC (2008).

Verfondern, K., Nabielek, H., PANAMA Ein Rechenprogramm zur Vorhersage des Partikelbruchanteils von TRISO-Partikeln unter Störfallbedingungen. Report Jül-Spez-298, Research Center Jülich (1985).

8 Annexes

Annex 1 –

Annex 2 – Title 2

IDENTIFICATION	REVISION
FS1-0016339	1.0

AREVA Front End BG
Fuel BU

AREVA

TOTAL NUMBER OF PAGES: 31

ARCHER - Calculation with ATLAS V3.0.3 of the HFR-EU1 irradiation on TRISO Fuel

ADDITIONAL INFORMATION:

PROJECT	ARCHER
HANDLING	Restricted AREVA
CATEGORY	TEP - Technical Report
STATUS	BPE

DISTRIBUTION TO	PURPOSE OF DISTRIBUTION
Marylise CARON-CHARLES	For information
Benoît WINTERHOLER	For information
Pierre GUILLERMIER	For information
Lucile DANIEL	For information
Nicolas JAMET	For information

This document is electronically approved. Records regarding the signatures are stored in the Fuel BU Document Database. Any attempt to modify this file may subject employees to civil and criminal penalties. EDM Object Id: 09012167805dc257 - Release date (YYYY/MM/DD) : 2015/01/20 17:58:16 [Western European Time]

Role	Name	Date (YYYY/MM/DD)	Organization
Writer	GAUTHIER Laurent	2015/01/20 12:14:40	FDM-F
Reviewer	DANIEL Lucile	2015/01/20 14:12:58	FDM-F
Approver	WINTERHOLER Benoit	2015/01/20 17:58:10	FDM-F

RELEASE DATA:

CHANGE CONTROL RECORDS:
This document, when revised, must be reviewed or approved by the following regions:

France:	Y
USA:	N
Germany:	N

Exportkennzeichnung AL: 0E001 ECCN: N
Die mit "AL ungleich N" gekennzeichneten Güter unterliegen bei der Ausfuhr aus der EU bzw. innergemeinschaftlichen Verbringung der europäischen bzw. deutschen Ausfuhrgenehmigungspflicht. Die mit "ECCN ungleich N" gekennzeichneten Güter unterliegen der US-Reexportgenehmigungspflicht. Auch ohne Kennzeichen, bzw. bei Kennzeichen "AL: N" oder "ECCN: N", kann sich eine Genehmigungspflicht, unter anderem durch den Endverbleib und Verwendungszweck der Güter, ergeben.

Export classification AL: 0E001 ECCN: N
Goods labeled with "AL not equal to N" are subject to European or German export authorization when being exported within or out of the EU. Goods labeled with "ECCN not equal to N" are subject to US reexport authorization. Even without a label, or with label "AL: N" or "ECCN: N", authorization may be required due to the final whereabouts and purpose for which the goods are to be used.

REVISIONS

REVISION	DATE	EXPLANATORY NOTES
1.0	See 1st page release date	New document

TABLE OF CONTENTS

LIST OF TABLES

LIST OF FIGURES

ABREVIATION

AVR	Arbeitsgemeinschaft Versuchsreaktor in Juelich
EFPD	Equivalent Full Power Day
FIMA	Fission rate per Initial Metal Atom
HFR	High Flux Reactor in Petten
SD	Standard Deviation
TC	ThermoCouple

REFERENCES

[1] Verfondern K., Xhonneux A., Nabielek H. and Allelein H.-J., Analysis of Modern HTGR Fuel Performance during the HFR-EU1 irradiation Test and Prediction of Fission Product Release in PIE Accident simulation testing, ICONE21-16694 (July 29-August 2, 2013)

[2] HTR-F1-04/08-D-3.1.1 Draft, Selection of Benchmark Cases for Mechanical Failure Prediction

[3] HFR-04-4786 Revision D, HFR-EU1 – Irradiation of AVR and INET High Temperature Reactor Fuel Pebbles to High Burn-Up in the HFR Petten – Design and Safety Report

[4] CEA SESC/LSC 09-018 Revision 0, 'RAPHAEL2008' - A reference set of Models and Properties for HTR fuel particle calculations with ATLAS V3.0

[5] HTR-F-01/07-D-2.1.1 Revision 4, Test Specification for the Irradiation Experiment HFR-EU1

[6] File “Fuetterer-HFR-EU1 BU evolution.xls”

[7] File “Fuetterer-Axial_Temp.xls”

[8] Verfondern K., Postcalculation Fuel Performance HFR-EU1, ARCHER Projet D3.2.13

[9] File “Fig 8-9 Copy of RoverB_vs_BU last version.xls

1. INTRODUCTION

This work is given in the framework of the European ARCHER project, where AREVA contribution is a fuel performance calculation of the HFR-EU1 experiment using the CEA/AREVA ATLAS V3.0.3 code. It has been chosen to focus on the comparison of calculated and experimental results for the Release-Over-Birth (RoB) of Xe-133, Kr-85m and Kr-88.

In this report are given the following data:

- In the first chapter are given the data of the HFR-EU1 experiment. A lot of these data are preliminary.
- In the second chapter, the chosen model assumptions for ATLAS are given. Some of these assumptions have been dedicated for the particular calculation of fast decaying isotopes.
- In the third chapter, the results of calculation are compared with experimental data and discussed.

2. DATA

2.1. APPARATUS

HFR-EU1 apparatus is shown in Figure 1. It consists of a total of 5 pebbles of 60 mm in diameter with LEU UO2 TRISO coated particles in two capsules:

- **INET Capsule:** 2 Chinese pebbles (HFR-EU1/1, HFR-EU1/2) manufactured by INET and taken from the fuel production for HTR-10 test reactor,
- **AVR Capsule:** 3 German pebbles (HFR-EU1/3, HFR-EU1/4, HFR-EU1/5) of type AVR GLE-4 for AVR reload 21-2 in October 1987, manufactured by HOBEG.

Axial position of elements relevant for current analysis are given in Table 1; axial position is given from core centerline which matches the center of the HFR-EU1/3 pebble.

2.2. FUEL CHARACTERISTICS

2.2.1. PEBBLES CHARACTERISTICS

Pebbles characteristics are given in Table 2.

2.3. PARTICLES CHARACTERISTICS

Particles characteristics are given in Table 3 for German particle batch HT 354-383.

2.4. LOAD

2.4.1. DURATION OF HFR CYCLES

HFR-EU1 was subjected to 16 HFR cycles, up to 444.9 EFPD; duration of each HFR cycles and cumulated time in equivalent full power days is given in Table 4.

The step time between cycles has been assumed, for model purpose, to last 2 days, with loads linearly interpolated between the loads of each cycle.

2.4.2. SURFACE TEMPERATURE

Temperature has been measured by 34 thermocouples (TC); axial location of theses TC and condition of contacts is given in Table 1. For each cycles is given in Table 5 the temperature for each of the TC groups, averaged with time and available TC in each group.

Temperature at the surface of each of the 5 pebbles is given in Table 6, along with the selected group of TC. As some TC were subjected to failure, some pebbles do not have a temperature up to the last cycle; it has been chosen to assume that the temperature in the missing cycles is equal to the last available measurement for each pebble.

2.4.3. POWER

Thermal power inside pebbles is composed of:

- fission power,
- gamma heating.

Fission power is calculated in a simplified fashion using the following formula:

(Eq. 1) $P_{f,i} = f_i \cdot E_f \cdot \frac{m_{HM}}{M_{HM}} \cdot K_A$ with $M_{HM} = 235 \cdot e_{235U} + 238 \cdot \left(1 - e_{235U}\right)$

Where:

$P_{f,i}$ $[\mathrm{W}]$ is the thermal power of the pebble from fission of the cycle i,

f_i $\left[\mathrm{s}^{-1}\right]$ is the mean fission rate of the cycle i (cf. §2.4.6),

$E_f = 200\,\mathrm{MeV}$ is the thermal energy per fission,

m_{HM} $[\mathrm{g}]$ is the heavy metal per pebble,

M_{HM} $\left[\mathrm{g \cdot mol^{-1}}\right]$ is the molar mass of the heavy metal,

K_A $\left[\mathrm{mol^{-1}}\right]$ is the Avogadro constant,

e_{235U} $[\mathrm{w\%}]$ is the enrichment in Uranium-235.

This formula may be written:

$$P_{f,i} = f_i \cdot K_P \text{ with } K_P = \begin{cases} 4.9 \cdot 10^{11}\ \mathrm{J} & \text{for AVR pebbles} \\ 4.1 \cdot 10^{11}\ \mathrm{J} & \text{for INET pebbles} \end{cases}$$

Calculated fission power is given in Table 8.

Gamma heating is assumed to be 3 $\mathrm{W.g^{-1}}$ and so about 5 $\mathrm{W.cm^{-3}}$.

2.4.4. TEMPERATURE INSIDE PEBBLES

Temperature field in the pebble is given by the following formula:

(Eq. 2) $$T_i(r) = \frac{P_i^v}{6 \cdot \lambda} \cdot \left(R_e{}^2 - r^2\right) + T_i(R_e)$$

Where:

R_e $[\mathrm{m}]$ is the external radius of the pebble (the external portion of the pebble without particles is neglected).

$T_i(r)$ $[\mathrm{K}]$ is the temperature at the radial abscissa r in the pebble during the cycle i.

P_i^v $\left[\mathrm{W \cdot m^{-3}}\right]$ is the volume power during the cycle i, as given in §2.4.3.

$\lambda = 20\ \mathrm{W \cdot m^{-1} \cdot K^{-1}}$ is the assumed thermal conductivity of the pebble.

Geometry of the pebble gives a triangular density function of the particles regarding temperature. This distribution cannot be handled in the statistical module of ATLAS. In order to handle this distribution, for each pebble, 3 calculations are done:

- One with the surface temperature (cf . §2.4.2),
- One with the center temperature, using (Eq. 2), given in Table 7,
- One with the mean temperature.

2.4.5. FAST NEUTRON FLUENCE

Calculated fast neutron fluence for each of the 5 pebbles is given in Table 9. Data are available only for HFR-EU1/1 and HFR-EU1/3. Fluence is almost proportional to burnup, so missing data for fluence is calculated the following way:

(Eq. 3) $$\Delta\Phi_i = \frac{\Delta BU_i}{C_{BU \to \Phi, i}}$$

Where:

$\Delta\Phi_i$ $\left[\mathrm{n \cdot m^{-2}\,(E > 0.1\,MeV)}\right]$ is the fluence increase during the cycle i,

ΔBU_i $[\mathrm{FIMA}]$ is the burnup increase during the cycle i,

$C_{BU \to \Phi, i}$ $\left[\left(\mathrm{n \cdot m^{-2}(E > 0.1\,MeV)}\right)^{-1}\right]$ is the proportionality coefficient from burnup to fluence for the cycle i, averaged between HFR-EU1/1 and HFR-EU1/3.

Calculated average neutron flux, which is the input data for ATLAS V3.0.3, is also given in Table 9.

2.4.6. BURNUP

Calculated burnup for each of the 5 pebbles is given in Table 10 at the end of each cycle. The relative fission rate, which is the input data for ATLAS V3.0.3, is given in Table 11; it is calculated the following way:

$$F_i = \frac{f_i}{\langle f_i \rangle} \text{ with } f_i = \frac{\Delta BU_i}{\Delta t_i}$$

Where:

F_i $[/]$ is the relative fission rate of the cycle i,

f_i $\left[\text{s}^{-1}\right]$ is the mean fission rate of the cycle i,

$\langle f_i \rangle$ $\left[\text{s}^{-1}\right]$ is the mean fission rate for all the cycles,

ΔBU_i $[\text{FIMA}]$ is the burnup increase during the cycle i,

Δt_i $[\text{s}]$ is the length of the cycle i.

2.5. IRRADIATION RESULTS

2.5.1. RELEASE-TO-BIRTH RATIO

Release-to-birth ratio is given:

- for INET capsule, in Table 12 and Table 13,
- for AVR capsule, in Table 14 and Table 15.

3. MODEL

3.1. MESH AND NUMERICAL PARAMETERS

The chosen mesh is the “pseudo”-1D mesh, most standard mesh in ATLAS. Number of elements par layer is given in Table 16, with time parameters for the ATLAS calculation.

3.2. GAPS INSIDE THE PARTICLE

It has been assumed that there is no gap inside the particle, between the kernel and the buffer, and between the buffer and the IPyC layer. Accordingly, to avoid parasitic mechanical effects, the Buffer Young’s Modulus has been fixed at 1 MPa [4].

3.3. MODELLING THE MATRIX

Matrix has an effect regarding the following phenomenon:

- Thermal diffusion: applied temperature is the calculated temperature inside the pebble, so the matrix is handled.
- Fission product diffusion: it is assumed that the matrix has no effect in terms of diffusion of fission products (high diffusivity inside matrix) and fission product storage.
- Mechanical interaction: it is assumed that no mechanical interaction with the matrix happens.

As written in [4], the matrix would not be modeled.

3.4. RELEASE FROM THE KERNEL

As written in [4], the release model from the Kernel will be connected.

3.5. AMOEBA EFFECT

As written in [4], amoeba effect model option is disconnected, due to the fact that it cannot be handled in 1D calculation.

3.6. PALLADIUM CORROSION OF THE SIC LAYER

Palladium corrosion model option is disconnected, due to the lack of quantitative results.

3.7. FIRST IMPERMEABLE LAYER

As written in [4], this option is disconnected.

3.8. RELEASE-TO-BIRTH CALCULATIONS

As written in [4], release-to-birth is calculated using a “ghost layer” with no mechanical effect. Its radius is 1000 µm, its porosity is 50%, and it is divided in 10 parts.

3.9. FISSION GAS RELEASE AND DECAY RATE

The following gas have been considered: xenon, krypton, carbon monoxide, carbon dioxide.

In order to avoid numerical problems (cf. §4.2), the decay of Xe-133, Kr-85m and Kr-88 has been disconnected in the two last dense layers (SiC and OPyC).

4. CALCULATIONS

4.1. RESULTS

Calculation and experimental results of Release-Over-Birth (RoB) are compared for the following cases:

- in Figure 2 for Xe-133,
- in Figure 3 for Kr-85m,
- in Figure 4 for Kr-88.

4.2. DISCUSSION

The following elements may be given:

- The calculated RoB is exceptionally good for Xe-133 with almost a null error, but gives a bad result for Kr-85m and Kr-88 with an almost 3 magnitude order difference; ATLAS has not been designed to model in a specific way Xe-133 disregarding Kr isotopes. **At least, it can be said that the specific used model is relevant for modeling of Xe-133 for the specific HFR-EU1 experiment**. Further studies should be done to assess this point.
- The 2 orders of magnitude increase of the RoB between the beginning and the end of the experimental is well calculated, but the shape of this increase shows some systematic (for the whole three isotopes) deviation: the calculation shows three phases: stability between 0%-4%FIMA, a steep increase between 4%-6%FIMA, and a stability (some decrease) between 6%FIMA and 14%FIMA. The experimental data show also an evolution of the rate of variation of the RoB, but these changes seem less steep and the RoB never decreases. The origin of these changes (temperatures, burnup or fluence data? release model?) should be assessed for further understanding.
- Calculations show little differences between different pebbles and different temperatures.
- The periodical pikes that may be seen for each plots are located at each shut-down of the HFR reactor.

This calculation of RoB of radioactive isotopes highlights some important difficulties that should be studied in detailed for further developments of ATLAS:

- The half-life of Xe-133, Kr-85m and Kr-88 are really short: less than one day. This means that the time step of numerical calculation should be also short to get an as accurate as possible calculation. Many time steps imply long calculation, and so it is not possible, with limited calculus capabilities, to make some statistical calculations.
- In some cases, especially after power changes, some numerical problems arise in the dense layers where the quantity of radioactive decaying products is too small and leads to numerical problems (numbers too small). That's why it has been chosen not to model the decay in the dense layers, only in the tank buffer layer, where is present the biggest inventory of these products. The impact of this assumption should be evaluated.

5. CONCLUSION

The calculation show a really good agreement of ATLAS calculation with experimental data of HFR-EU1 for Release-Over-Birth (RoB) of Xe-133, but a poor agreement for Kr-85m and Kr-88.

Altogether, calculation of fast decaying fission products is not easy to handle by numeric methods, and further studies of input data and model assumption should reinforce present results.

Table 1: HFR-EU1 Apparatus axial disposition

Axial position [mm]	Object	Comment
~ +237	Top of HFR-EU1/1	
+236 [7]	TC1, 2	TC in contact with HFR-EU1/1 surface
+228 [7]	TC3, 4, 5, 6	TC in contact with HFR-EU1/1 surface
+207 [3]	Center of HFR-EU1/1	INET pebble
~ +177	Bottom of HFR-EU1/1	
+173 [7]	TC7, 8	TC in holders gap
~ +167	Top of HFR-EU1/2	
+159 [7]	TC9, 10, 11, 12	TC in contact with HFR-EU1/2 surface
+137 [3]	Center of HFR-EU1/2	INET pebble
~ +107	Bottom of HFR-EU1/2	
+102 [7]	TC13, 14	TC in holders gap
+35 [7]	TC15, 16	TC in holders gap
~ +30	Top of HFR-EU1/3	
0 [3]	Center of HFR-EU1/3 Core centerline	AVR Pebble
-22 [7]	TC17, 18, 19, 20	Contact with HFR-EU1/3 surface
~ -30	Bottom of HFR-EU1/3	
-35 [7]	TC21, 22	TC in holders gap
~ -40	Top of HFR-EU1/4	
-70 [3]	Center of HFR-EU1/4	AVR Pebble
-91 [7]	TC23, 24, 25, 26	TC in contact with HFR-EU1/4 surface
~ -100	Bottom of HFR-EU1/4	
-105 [7]	TC27, 28	TC in holders gap
~ -110	Top of HFR-EU1/5	
-140 [3]	Center of HFR-EU1/5	AVR Pebble
-160 [7]	TC29, 30, 31, 32	TC in contact with HFR-EU1/5 surface
-168 [7]	TC33, 34	TC in contact with HFR-EU1/5 surface
~ -170	Bottom of HFR-EU1/5	

orange: calculation (approximate)
Axial position is given in mm from core centerline.

Table 2: Characteristics of the pebbles of HFR-EU1

Pebble		**AVR**	**INET**
Manufacturer		HOBEG	INET
Origin		Germany	China
Fuel type		AVR GLE 4-2	HTR-10
Particle batch		HT 385-393 HT 395-404 HT 406-423	
Kernel type		UO2 LEU	UO2 LEU
Heavy metal loading per pebble	[g]	6.0 [5]	5.02 [5]
U-235 content per pebble	[g]	1.00 ± 1% [5]	0.858 [5]
Diameter	[mm]	60 [3]	60 [3]
Active zone diameter	[mm]	~47 [3]	~47 [3]
Number of particles per sphere	-	9560 [3]	8500 [3]
Volume packing fraction	[/]	6.2% [3]	5.0% [3]
Matrix graphite grade	-	A3-3 [3]	A3-3 [3]
Final heat treatment temperature	[°C]	1900 [5]	
Matrix density	[$g.cm^{-3}$]	1.75 [5]	1.76 [3]
Defective SiC layers	[U/U_{tot}]	$7.8*10^{-6}$ [5]	$2.3*10^{-7}$ [5]

Table 3: Characteristics of a typical German AVR particle batch

Layer	Parameter	Unit	Average	SD
Kernel	Diameter	[µm]	502.2 [2]	10.6 [2]
	Radius	[µm]	251.1	5.3
	Density	[g.cm-3]	10.86 [2]	
	Theoretical density	[g.cm-3]	10.93 [4]	
	Porosity	[%]	0.64%	
	Open porosity	[%]	1%	
	Grain size	[µm]	10	
	U235 Content	[w%]	16.76 [3]	
	O/M	[/]	2.00	
Buffer	Kernel-Buffer gap	[µm]	*no gap*[1]	
	Thickness	[µm]	94.3 [3]	13.0 [2]
	Buffer-IPyC gap	[µm]	*no gap*[1]	
	Density	[g.cm-3]	1.012 [2]	
	Theoretical density	[g.cm-3]	2.209 [4]	
	Porosity	[%]	54.2%	
	Open porosity	[%]	100%[1]	
Inner PyC	Thickness	[µm]	40.6 [2]	3.7 [2]
	Density	[g.cm-3]	1.87 [2]	
	Theoretical density	[g.cm-3]	2.209 [4]	
	Porosity	[%]	15.4 %	
	Anisotropy (BAF)	[/]	1.02 [2]	
SiC	Thickness	[µm]	35.9 [2]	2.2 [2]
	Density	[g.cm-3]	3.20 [2]	
	Theoretical density	[g.cm-3]	3.233 [4]	
	Porosity	[%]	1.0 %	
Outer PyC	Thickness	[µm]	39.8 [2]	3.3 [2]
	Density	[g.cm-3]	1.87 [2]	
	Theoretical density	[g.cm-3]	2.209 [4]	
	Porosity	[%]	15.4 %	
	Anisotropy (BAF)	[/]	1.02 [2]	

SD: Standard Deviation
blue: model assumption
orange: calculation

[1] As recommended by the RAPHAEL2008 set of laws and models

Table 4: Duration of the HFR cycles in EPFD

HFR cycle	Cumulated time	Cycle duration	Inter-cycle time
06-08	24.2 [1]	24.2	2
06-09	51.1 [1]	26.9	2
06-10	79.7 [1]	28.6	2
07-01	107.5 [1]	27.8	2
07-02	136.4 [1]	28.9	2
07-03	164.3 [1]	27.9	2
07-07	191.2 [1]	26.9	2
07-08	220.4 [1]	29.2	2
07-09	248.4 [1]	28.0	2
07-10	276.2 [1]	27.8	2
08-01	304.0 [1]	27.8	2
08-02	332.8 [1]	28.8	2
09-08	357.6 [1]	24.8	2
09-09	389.0 [1]	31.4	2
09-10	413.2 [1]	24.2	2
10-01	444.9 [1]	31.7	2

Time is given in EFPD (**e**quivalent **f**ull **p**ower **d**ay)
Inter-cycle time is given in days
orange: calculation
blue: model assumption (to be subtracted from cycle duration)

Table 5: Temperature for each set of thermocouple

TC group	TC1 TC2	TC3 TC4 TC5 TC6	TC9 TC10 TC11 TC12	?	TC13 TC14	TC15 TC16	TC17 TC18 TC19 TC20	TC21 TC22	TC23 TC24 TC25 TC26	TC27 TC28	TC29 TC30 TC31 TC32	TC33 TC34
Axial position	**236**	**228**	**173**	**159**	**102**	**35**	**-22**	**-35**	**-91**	**-105**	**-160**	**-168**
06-08	804	800	905	901	897	962	946	963	969	984	965	969
06-09	836	832	919	923	919	939	926	945	949	966	938	938
06-10	825	820	936	929	921	954	939	914	953	972	931	938
07-01	865	851	946	941	963	960	929	N/A	946	974	930	955
07-02	854	840	943	933	961	N/A	951	N/A	957	986	956	984
07-03	835	821	946	939	974	N/A	930	N/A	945	973	951	977
07-07	847	828	953	933	970	N/A	933	N/A	936	957	926	955
07-08	833	810	975	948	994	N/A	936	N/A	949	966	942	974
07-09	863	831	N/A	924	984	N/A	948	N/A	941	956	934	958
07-10	842	819	N/A	944	1000	N/A	N/A	N/A	941	941	981	996
08-01	867	839	N/A	926	982	N/A	N/A	N/A	949	969	N/A	977
08-02	879	849	N/A	943	1007	N/A	N/A	N/A	936	N/A	N/A	988
09-08	836	810	910	901	N/A	N/A	N/A	N/A	N/A	N/A	N/A	980
09-09	884	864	N/A	942	N/A	N/A	N/A	N/A	N/A	N/A	N/A	986
09-10	850	833	N/A	931	N/A	N/A	N/A	N/A	N/A	N/A	N/A	987
10-01	896	873	N/A	943	N/A	N/A	N/A	N/A	N/A	N/A	N/A	988

Axial position is given in mm from centerline.
Temperature is given in °C. It's the average of the temperature given by the available thermocouples in each axial position.
Reference: [7]

Table 6: Averaged measured surface temperature for each pebble

HFR cycle	HFR-EU1/1 (INET)	HFR-EU1/2 (INET)	HFR-EU1/3 (AVR)	HFR-EU1/4 (AVR)	HFR-EU1/5 (AVR)
TC group	TC3 TC4 TC5 TC6	TC9 TC10 TC11 TC12	TC17 TC18 TC19 TC20	TC23 TC24 TC25 TC26	TC29 TC30 TC31 TC32
06-08	800	905	946	969	965
06-09	832	919	926	949	938
06-10	820	936	939	953	931
07-01	851	946	929	946	930
07-02	840	943	951	957	956
07-03	821	946	930	945	951
07-07	828	953	933	936	926
07-08	810	975	936	949	942
07-09	831	975	948	941	934
07-10	819	975	948	941	981
08-01	839	975	948	949	981
08-02	849	975	948	936	981
09-08	810	910	948	936	981
09-09	864	910	948	936	981
09-10	833	910	948	936	981
10-01	873	910	948	936	981

Temperature is given in °C. Data come from Table 5.
violet: assumption for missing data

Table 7: Calculated center temperature for each pebble

HFR cycle	HFR-EU1/1 (INET)	HFR-EU1/2 (INET)	HFR-EU1/3 (AVR)	HFR-EU1/4 (AVR)	HFR-EU1/5 (AVR)
06-08	1172	1293	1378	1402	1389
06-09	1202	1305	1353	1379	1359
06-10	1189	1320	1362	1377	1349
07-01	1223	1336	1357	1377	1350
07-02	1212	1332	1377	1387	1375
07-03	1191	1333	1351	1370	1366
07-07	1220	1367	1394	1403	1383
07-08	1200	1389	1393	1411	1395
07-09	1220	1385	1398	1396	1381
07-10	1205	1380	1391	1388	1421
08-01	1223	1376	1383	1388	1414
08-02	1231	1372	1376	1368	1408
09-08	1190	1304	1370	1362	1402
09-09	1242	1301	1364	1356	1397
09-10	1209	1298	1360	1351	1392
10-01	1247	1295	1354	1345	1387

Temperature is given in °K. Calculated according to Eq. 2 p. 7.
orange: calculation

Table 8: Fission thermal power per pebble

HFR cycle	HFR-EU1/1 (INET)	HFR-EU1/2 (INET)	HFR-EU1/3 (AVR)	HFR-EU1/4 (AVR)	HFR-EU1/5 (AVR)
06-08	890	1130	1791	1815	1672
06-09	867	1099	1727	1760	1637
06-10	843	1078	1657	1683	1580
07-01	898	1164	1735	1789	1617
07-02	898	1150	1700	1761	1600
07-03	863	1114	1636	1696	1536
07-07	1189	1528	2237	2321	2174
07-08	1166	1526	2175	2257	2115
07-09	1146	1463	2075	2150	2031
07-10	1111	1394	1957	2024	1923
08-01	1074	1330	1842	1904	1815
08-02	1038	1274	1737	1794	1715
09-08	1008	1226	1649	1701	1632
09-09	977	1178	1564	1611	1550
09-10	953	1137	1493	1536	1483
10-01	918	1084	1411	1449	1404

Power is given in W.
orange: calculation according to §2.4.3

Table 9: Calculated fast neutron fluence in the pebbles at the end of each cycle and average neutron flux

HFR cycle	HFR-EU1/1 (INET)	HFR-EU1/2 (INET)	HFR-EU1/3 (AVR)	HFR-EU1/4 (AVR)	HFR-EU1/5 (AVR)
06-08	0.099	0.12	0.156	0.16	0.15
06-09	0.21	0.26	0.332	0.35	0.32
06-10	0.399	0.50	0.63	0.66	0.61
07-01	0.588	0.74	0.929	0.97	0.89
07-02	0.793	1.00	1.252	1.30	1.20
07-03	0.988	1.25	1.56	1.62	1.49
07-07	1.158	1.47	1.829	1.90	1.75
07-08	1.422	1.82	2.246	2.33	2.15
07-09	1.64	2.10	2.589	2.68	2.48
07-10	1.848	2.37	2.918	3.01	2.79
08-01	2.053	2.64	3.241	3.33	3.10
08-02	2.278	2.93	3.597	3.67	3.43
09-08	2.468	3.18	3.897	3.96	3.70
09-09	2.711	3.49	4.281	4.32	4.05
09-10	2.896	3.74	4.573	4.59	4.31
10-01	3.135	4.05	4.95	4.94	4.65

Fast neutron fluence is given in 10^{25} $n.m^{-2}$ (E>0.1 MeV).
orange: approximate calculation
Reference: [8]

HFR-EU1/1 (INET)	HFR-EU1/2 (INET)	HFR-EU1/3 (AVR)	HFR-EU1/4 (AVR)	HFR-EU1/5 (AVR)
0.82	1.05	1.29	1.29	1.21

Neutron flux is given in 10^{18} $n.m^{-2}.s^{-1}$ (E>0.1 MeV).
orange: approximate calculation

Table 10: Burnup in the pebbles at the end of each cycle

HFR cycle	HFR-EU1/1 (INET)	HFR-EU1/2 (INET)	HFR-EU1/3 (AVR)	HFR-EU1/4 (AVR)	HFR-EU1/5 (AVR)
06-08	0.454%	0.576%	0.764%	0.775%	0.714%
06-09	0.945%	1.199%	1.583%	1.610%	1.490%
06-10	1.453%	1.849%	2.419%	2.458%	2.287%
07-01	1.980%	2.531%	3.270%	3.335%	3.079%
07-02	2.527%	3.231%	4.136%	4.232%	3.895%
07-03	3.034%	3.886%	4.941%	5.067%	4.650%
07-07	3.708%	4.753%	6.002%	6.168%	5.681%
07-08	4.425%	5.692%	7.122%	7.330%	6.771%
07-09	5.102%	6.555%	8.146%	8.391%	7.773%
07-10	5.753%	7.372%	9.105%	9.383%	8.716%
08-01	6.382%	8.151%	10.008%	10.316%	9.605%
08-02	7.012%	8.924%	10.890%	11.227%	10.476%
09-08	7.539%	9.565%	11.612%	11.971%	11.190%
09-09	8.186%	10.344%	12.477%	12.863%	12.048%
09-10	8.672%	10.924%	13.114%	13.518%	12.681%
10-01	9.285%	11.648%	13.903%	14.328%	13.465%

Burnup is given in %FIMA.
Reference: [6]

Table 11: Relative fission rate in the pebbles during each cycle

HFR cycle	HFR-EU1/1 (INET)	HFR-EU1/2 (INET)	HFR-EU1/3 (AVR)	HFR-EU1/4 (AVR)	HFR-EU1/5 (AVR)
06-08	90%	91%	101%	99%	97%
06-09	88%	88%	97%	96%	95%
06-10	85%	87%	93%	92%	92%
07-01	91%	94%	98%	98%	94%
07-02	91%	93%	96%	96%	93%
07-03	87%	90%	92%	93%	89%
07-07	120%	123%	126%	127%	127%
07-08	118%	123%	123%	123%	123%
07-09	116%	118%	117%	118%	118%
07-10	112%	112%	110%	111%	112%
08-01	108%	107%	104%	104%	106%
08-02	105%	103%	98%	98%	100%
09-08	102%	99%	93%	93%	95%
09-09	99%	95%	88%	88%	90%
09-10	96%	92%	84%	84%	86%
10-01	93%	87%	80%	79%	82%
Mean fission rate	2.415e-9	3.030e-9	3.621e-9	3.731e-9	3.505e-9

Burnup is given in %FIMA.
Fission rate is given in s^{-1}.
orange: calculation as given in §2.4.6.

Table 12: Release-to-birth rate of gaseous fission products for INET Capsule (1/2)

Irradiation time	Burn-up	Kr-85m	Kr-87	Kr-88	Xe-133	Xe-135
8.4	0.2%	N/A	N/A	N/A	N/A	N/A
13.3	0.3%	1.3E-09	5.5E-10	9.8E-10	N/A	6.9E-10
21.5	0.5%	2.6E-09	N/A	2.5E-09	N/A	N/A
31.4	0.7%	1.7E-09	9.0E-10	1.2E-09	2.7E-09	5.9E-10
42.3	0.9%	2.1E-09	1.7E-09	N/A	N/A	1.4E-09
49.2	1.0%	3.7E-09	1.6E-09	3.2E-09	3.9E-09	1.2E-09
52.9	1.1%	3.2E-08	1.2E-08	2.1E-08	4.3E-07	9.8E-08
60.8	1.3%	4.6E-09	1.9E-09	2.0E-09	N/A	1.1E-09
66.9	1.4%	5.8E-09	2.5E-09	3.8E-09	5.1E-09	2.0E-09
84.7	1.7%	8.1E-08	3.1E-08	5.0E-08	1.2E-06	2.1E-07
98.8	2.1%	1.1E-08	5.0E-09	8.0E-09	1.6E-08	3.2E-09
105.7	2.2%	1.5E-08	6.0E-09	9.4E-09	1.4E-08	3.4E-09
116.6	2.5%	1.3E-07	5.1E-08	9.0E-08	2.2E-06	3.6E-07
123.6	2.6%	1.3E-08	6.1E-09	9.6E-09	9.7E-09	3.7E-09
131.7	2.8%	1.8E-08	8.4E-09	1.4E-08	1.7E-08	4.8E-09
138.4	2.9%	1.7E-08	8.8E-09	1.2E-08	N/A	4.3E-09
151.4	3.2%	2.0E-08	8.6E-09	1.3E-08	2.3E-08	4.9E-09
158.5	3.3%	1.8E-08	8.8E-09	1.3E-08	1.9E-08	4.1E-09
169.9	3.6%	2.0E-08	9.1E-09	1.4E-08	1.7E-08	4.6E-09
178.0	3.8%	2.0E-08	8.7E-09	1.3E-08	1.4E-08	4.2E-09
184.0	4.0%	2.1E-08	9.3E-09	1.5E-08	2.4E-08	4.5E-09
197.6	4.4%	2.1E-08	9.6E-09	1.5E-08	2.0E-08	4.5E-09
209.6	4.8%	2.5E-08	1.1E-08	1.7E-08	1.9E-08	5.1E-09
216.6	4.9%	2.5E-08	1.1E-08	1.7E-08	2.9E-08	5.0E-09
225.6	5.2%	1.9E-08	9.0E-09	1.3E-08	2.0E-08	4.3E-09
234.6	5.5%	2.0E-08	8.3E-09	1.3E-08	2.3E-08	4.3E-09
239.6	5.6%	2.0E-08	9.3E-09	1.4E-08	2.2E-08	4.7E-09
246.6	5.8%	2.6E-08	1.1E-08	1.7E-08	2.7E-08	5.2E-09
253.4	6.0%	2.0E-08	6.7E-09	1.3E-08	2.3E-08	4.6E-09
256.7	6.0%	1.9E-08	5.1E-09	1.1E-08	2.1E-08	4.2E-09
265.5	6.3%	2.9E-08	5.8E-09	1.4E-08	3.7E-08	6.4E-09
272.6	6.5%	1.8E-08	4.9E-09	1.0E-08	2.1E-08	4.7E-09

Irradiation time is in EFPD
Burnup is in %FIMA
Release-to-birth ratio is in at/at.
Reference: [9]

Table 13: Release-to-birth rate of gaseous fission products for INET Capsule (2/2)

Irradiation	Burn-up	Kr-85m	Kr-87	Kr-88	Xe-133	Xe-135
285.1	6.8%	1.3E-08	3.1E-09	7.5E-09	2.0E-08	4.1E-09
292.2	7.0%	1.5E-08	3.8E-09	8.7E-09	1.8E-08	4.2E-09
298.3	7.1%	2.6E-08	1.2E-08	1.8E-08	2.5E-08	5.4E-09
303.2	7.2%	2.6E-08	1.2E-08	1.8E-08	2.4E-08	5.1E-09
306.9	7.3%	3.2E-08	1.5E-08	2.2E-08	2.4E-08	6.6E-09
314.9	7.5%	3.1E-08	1.3E-08	2.1E-08	2.7E-08	5.9E-09
320.9	7.7%	3.7E-08	1.6E-08	2.5E-08	2.7E-08	6.8E-09
327.9	7.9%	3.7E-08	1.7E-08	2.7E-08	3.4E-08	6.8E-09
341.8	8.2%	3.4E-08	1.5E-08	2.4E-08	2.6E-08	6.4E-09
350.6	8.4%	3.2E-08	1.4E-08	2.1E-08	2.6E-08	6.1E-09
355.8	8.5%	3.4E-08	1.5E-08	2.4E-08	2.6E-08	6.3E-09
359.2	8.6%	3.5E-08	1.6E-08	2.5E-08	1.5E-08	7.5E-09
372.3	8.9%	3.8E-08	1.7E-08	2.7E-08	2.2E-08	7.2E-09
380.2	9.1%	4.2E-08	1.9E-08	2.9E-08	3.9E-08	7.9E-09
385.3	9.2%	4.5E-08	2.0E-08	3.1E-08	2.4E-08	8.5E-09
404.5	9.6%	4.6E-08	2.1E-08	3.2E-08	3.1E-08	9.6E-09
412.6	9.8%	4.5E-08	2.2E-08	3.1E-08	3.9E-08	8.7E-09
420.1	9.9%	5.2E-08	2.4E-08	3.6E-08	4.3E-08	1.1E-08
428.2	10.1%	5.4E-08	2.6E-08	3.9E-08	4.0E-08	1.1E-08
436.2	10.3%	6.8E-08	3.3E-08	5.1E-08	5.4E-08	1.3E-08
442.2	10.4%	7.2E-08	3.4E-08	5.0E-08	4.9E-08	1.4E-08

Irradiation time is in EFPD
Burnup is in %FIMA
Release-to-birth ratio is in at/at.
Reference: [9]

Table 14: Release-to-birth rate of gaseous fission products for AVR Capsule (1/2)

Irradiation time	Burn-up	Kr-85m	Kr-87	Kr-88	Xe-133	Xe-135
11.3	0.4%	N/A	1.2E-09	N/A	N/A	4.7E-10
14.4	0.4%	4.2E-09	1.8E-09	2.9E-09	4.0E-09	8.3E-10
22.4	0.7%	4.0E-09	2.0E-09	2.7E-09	N/A	9.3E-10
32.4	1.0%	3.3E-09	1.9E-09	3.1E-09	N/A	8.9E-10
43.3	1.3%	4.0E-08	1.6E-08	2.7E-08	4.4E-07	1.0E-07
50.4	1.5%	4.7E-09	2.3E-09	3.6E-09	N/A	8.4E-10
53.9	1.6%	6.8E-09	3.4E-09	5.0E-09	3.9E-09	1.5E-09
61.7	1.9%	8.1E-08	3.0E-08	5.5E-08	8.2E-07	1.7E-07
67.9	2.1%	9.3E-09	4.4E-09	6.6E-09	9.6E-09	1.6E-09
85.7	2.6%	1.8E-08	8.0E-09	1.3E-08	1.2E-08	2.3E-09
99.7	3.0%	2.3E-07	8.4E-08	1.5E-07	1.9E-06	3.0E-07
106.7	3.2%	2.6E-08	1.2E-08	1.8E-08	1.7E-08	3.6E-09
118.7	3.6%	3.7E-08	1.7E-08	2.5E-08	2.7E-08	4.1E-09
124.6	3.7%	3.9E-08	1.7E-08	2.7E-08	1.8E-08	4.6E-09
130.6	3.9%	4.2E-08	1.8E-08	2.8E-08	2.5E-08	4.5E-09
142.5	4.3%	4.4E-08	2.0E-08	3.1E-08	1.9E-08	4.9E-09
152.4	4.5%	3.9E-08	1.7E-08	2.7E-08	2.0E-08	4.6E-09
159.4	4.7%	4.2E-08	1.9E-08	3.0E-08	2.2E-08	4.4E-09
171.0	5.1%	5.3E-08	2.3E-08	3.7E-08	2.5E-08	4.8E-09
180.0	5.5%	5.2E-08	2.3E-08	3.7E-08	2.4E-08	5.1E-09
189.9	5.9%	5.3E-08	2.3E-08	3.6E-08	2.8E-08	4.7E-09
200.6	6.3%	6.3E-08	2.8E-08	4.4E-08	3.3E-08	6.1E-09
211.6	6.7%	6.9E-08	3.0E-08	4.9E-08	3.4E-08	6.5E-09
218.6	7.0%	5.3E-08	2.3E-08	3.7E-08	2.8E-08	5.3E-09
226.7	7.3%	6.8E-08	3.0E-08	4.8E-08	3.2E-08	7.0E-09
232.6	7.5%	6.1E-08	2.7E-08	4.1E-08	2.7E-08	6.2E-09
240.6	7.8%	6.3E-08	2.8E-08	4.4E-08	3.3E-08	6.6E-09
251.5	8.2%	9.6E-08	4.5E-08	6.9E-08	3.7E-08	8.9E-09
256.5	8.4%	6.3E-08	1.5E-08	3.6E-08	4.6E-08	8.2E-09
263.5	8.6%	7.2E-08	2.0E-08	4.3E-08	4.9E-08	8.5E-09
270.5	8.9%	7.6E-08	1.9E-08	4.5E-08	5.2E-08	8.9E-09
284.4	9.3%	8.6E-08	2.7E-08	5.4E-08	5.5E-08	1.1E-08

Irradiation time is in EFPD
Burnup is in %FIMA
Release-to-birth ratio is in at/at.
Reference: [9]

Table 15: Release-to-birth rate of gaseous fission products for AVR Capsule (2/2)

Irradiation time	Burn-up	Kr-85m	Kr-87	Kr-88	Xe-133	Xe-135
290.2	9.5%	7.0E-08	1.9E-08	4.2E-08	4.8E-08	9.8E-09
296.2	9.7%	8.6E-08	2.7E-08	5.5E-08	5.4E-08	1.2E-08
299.3	9.8%	1.1E-07	5.4E-08	8.4E-08	4.8E-08	1.3E-08
303.3	N/A	5.2E-08	2.9E-08	4.0E-08	3.0E-08	1.0E-08
312.9	10.3%	1.4E-07	7.1E-08	1.0E-07	6.4E-08	1.6E-08
316.9	10.4%	1.5E-07	7.7E-08	1.1E-07	7.0E-08	1.7E-08
322.9	10.6%	1.4E-07	7.0E-08	1.0E-07	7.0E-08	1.7E-08
328.9	10.7%	1.8E-07	9.1E-08	1.3E-07	7.4E-08	2.0E-08
339.6	11.1%	1.6E-07	8.3E-08	1.2E-07	5.7E-08	2.0E-08
348.7	11.3%	1.6E-07	8.2E-08	1.2E-07	6.6E-08	1.9E-08
354.8	11.5%	1.8E-07	9.0E-08	1.3E-07	7.5E-08	2.2E-08
360.3	11.7%	1.6E-07	8.3E-08	1.2E-07	5.6E-08	2.1E-08
367.2	11.9%	1.6E-07	8.9E-08	1.2E-07	6.5E-08	2.0E-08
374.1	12.1%	1.8E-07	9.7E-08	1.4E-07	7.8E-08	2.5E-08
379.0	12.2%	2.0E-07	1.1E-07	1.5E-07	8.2E-08	2.6E-08
386.3	12.4%	2.0E-07	1.1E-07	1.5E-07	8.1E-08	2.8E-08
403.5	12.9%	2.2E-07	1.2E-07	1.6E-07	9.2E-08	3.1E-08
410.5	13.0%	2.4E-07	1.3E-07	1.9E-07	9.4E-08	3.3E-08
420.0	13.3%	2.1E-07	1.2E-07	1.7E-07	8.8E-08	3.0E-08
427.0	13.5%	2.4E-07	1.4E-07	1.9E-07	8.7E-08	3.4E-08
431.0	13.6%	2.5E-07	1.4E-07	1.9E-07	8.8E-08	3.5E-08
441.0	13.8%	2.6E-07	1.5E-07	2.0E-07	1.2E-07	3.7E-08
444.1	13.9%	2.5E-07	1.4E-07	2.0E-07	9.4E-08	3.6E-08

Irradiation time is in EFPD
Burnup is in %FIMA
Release-to-birth ratio is in at/at.
Reference: [9]

Table 16: Number of mesh elements in the calculation

Mesh geometrical parameters		
Layer	**Parameter**	**Value**
Kernel	Number of radial element	5
Buffer	Number of radial element	3
Inner PyC	Number of radial element	5
SiC	Number of radial element	5
Outer PyC	Number of radial element	5
Overall	Number of angular element	12

Figure 1 : HFR-EU1 Apparatus

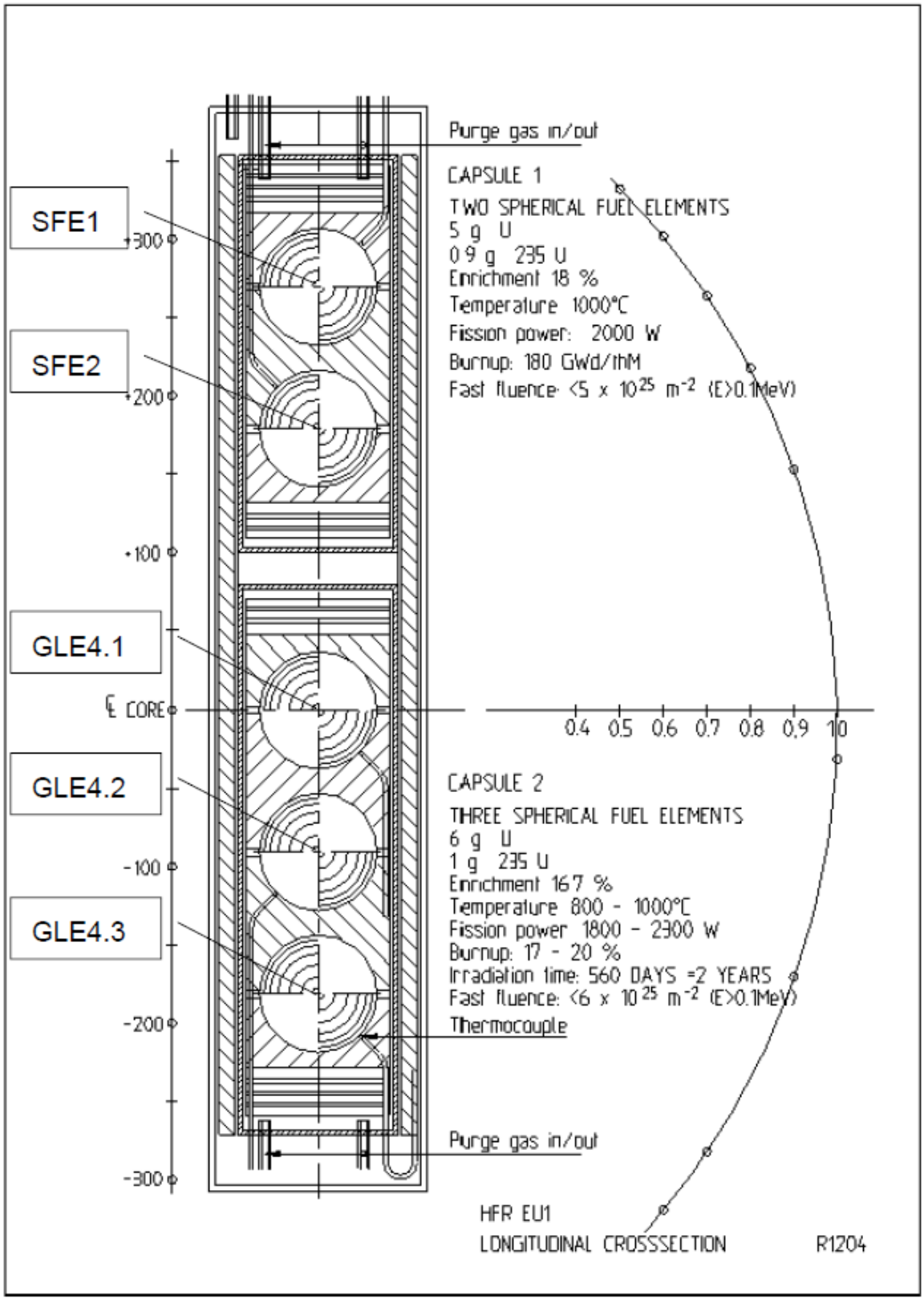

Figure 2 : Release-to-birth rate of Xe-133

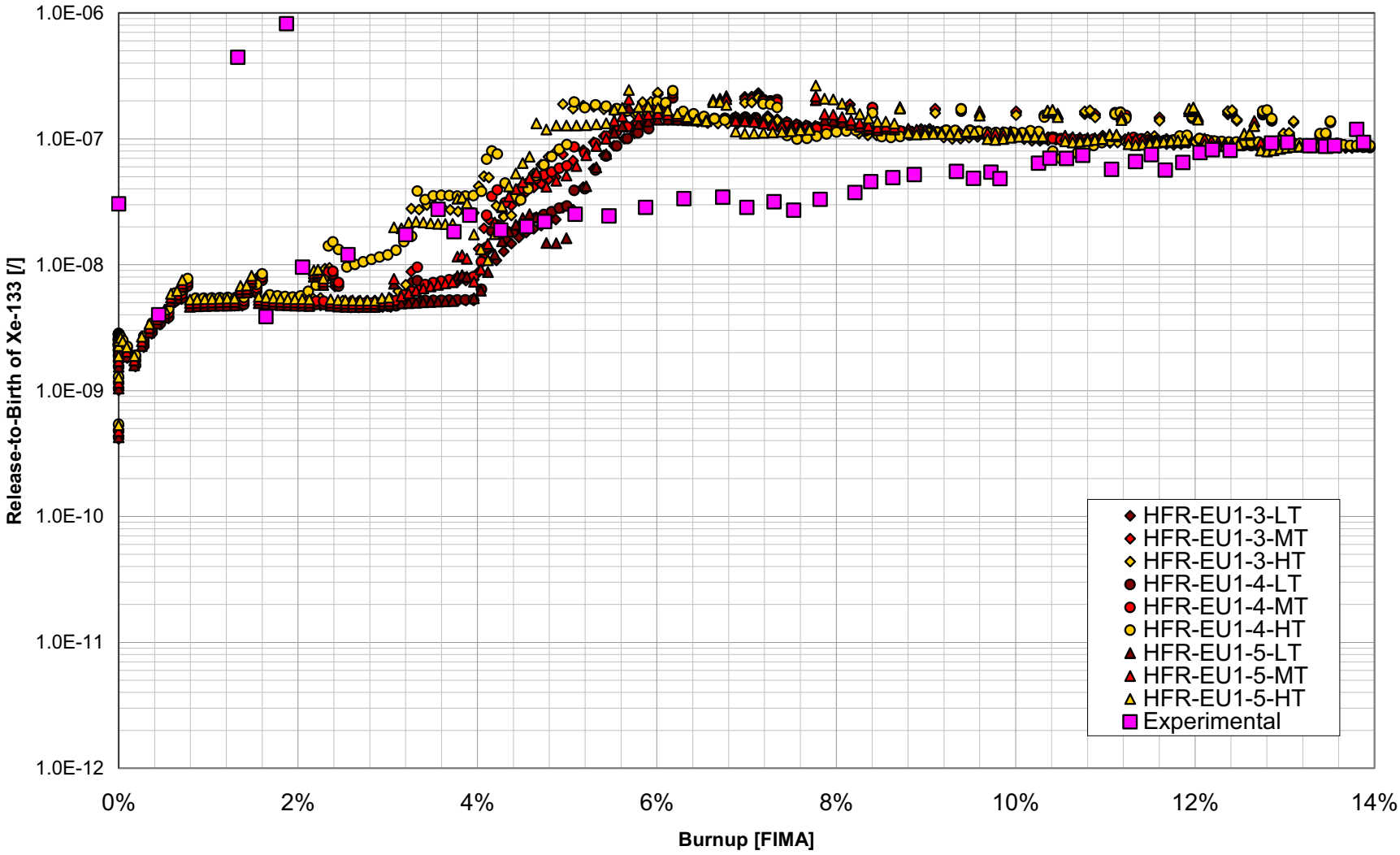

HFR-EU1-X-YY means calculation of the X pebble, with YY temperature condition (LT : Low, surface, Temperature ; MT : Mean temperature ; HT : High, center, temperature).

Figure 3 : Release-to-birth rate of Kr-85m

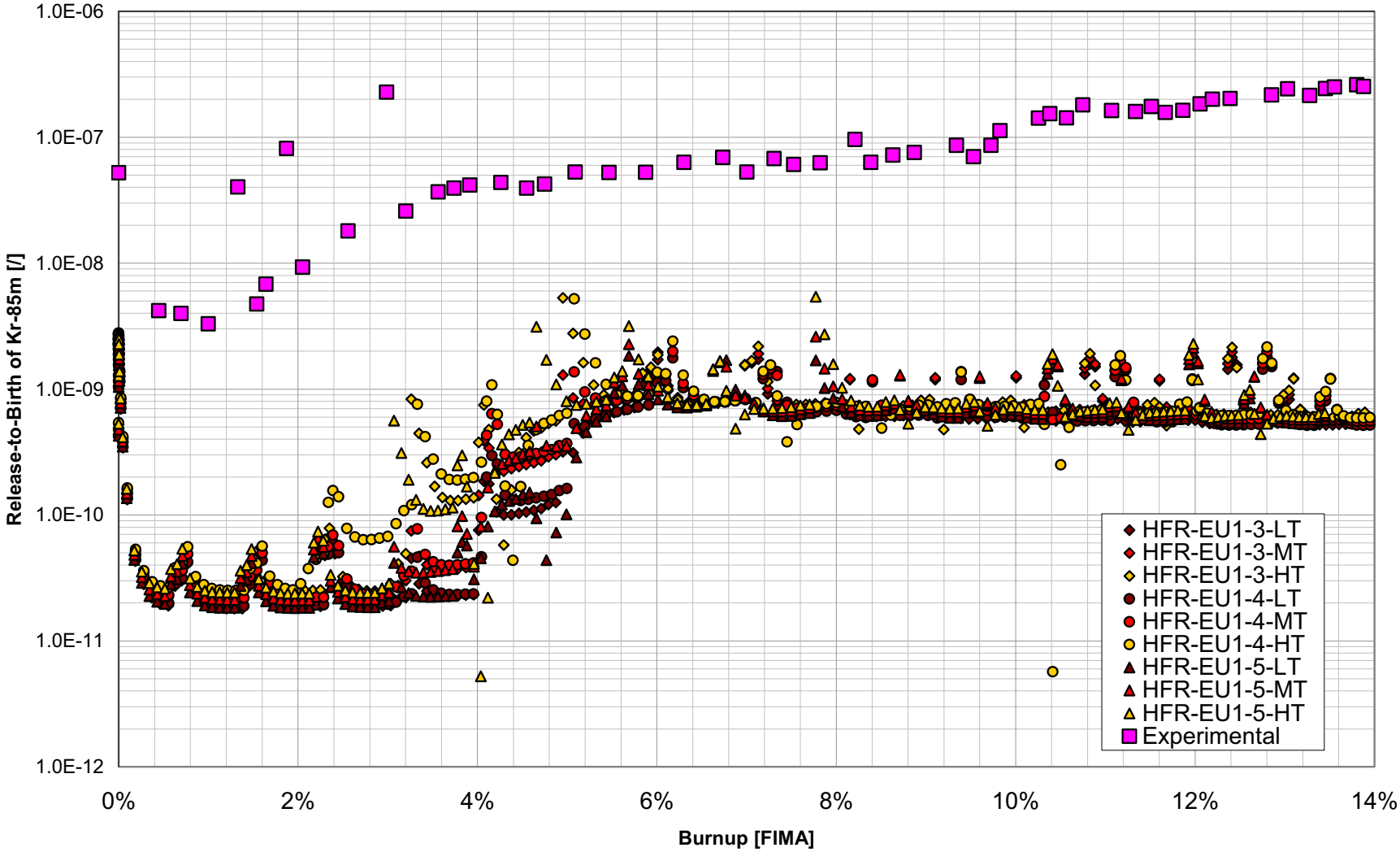

HFR-EU1-X-YY means calculation of the X pebble, with YY temperature condition (LT : Low, surface, Temperature ; MT : Mean temperature ; HT : High, center, temperature).

Figure 4 : Release-to-birth rate of Kr-88

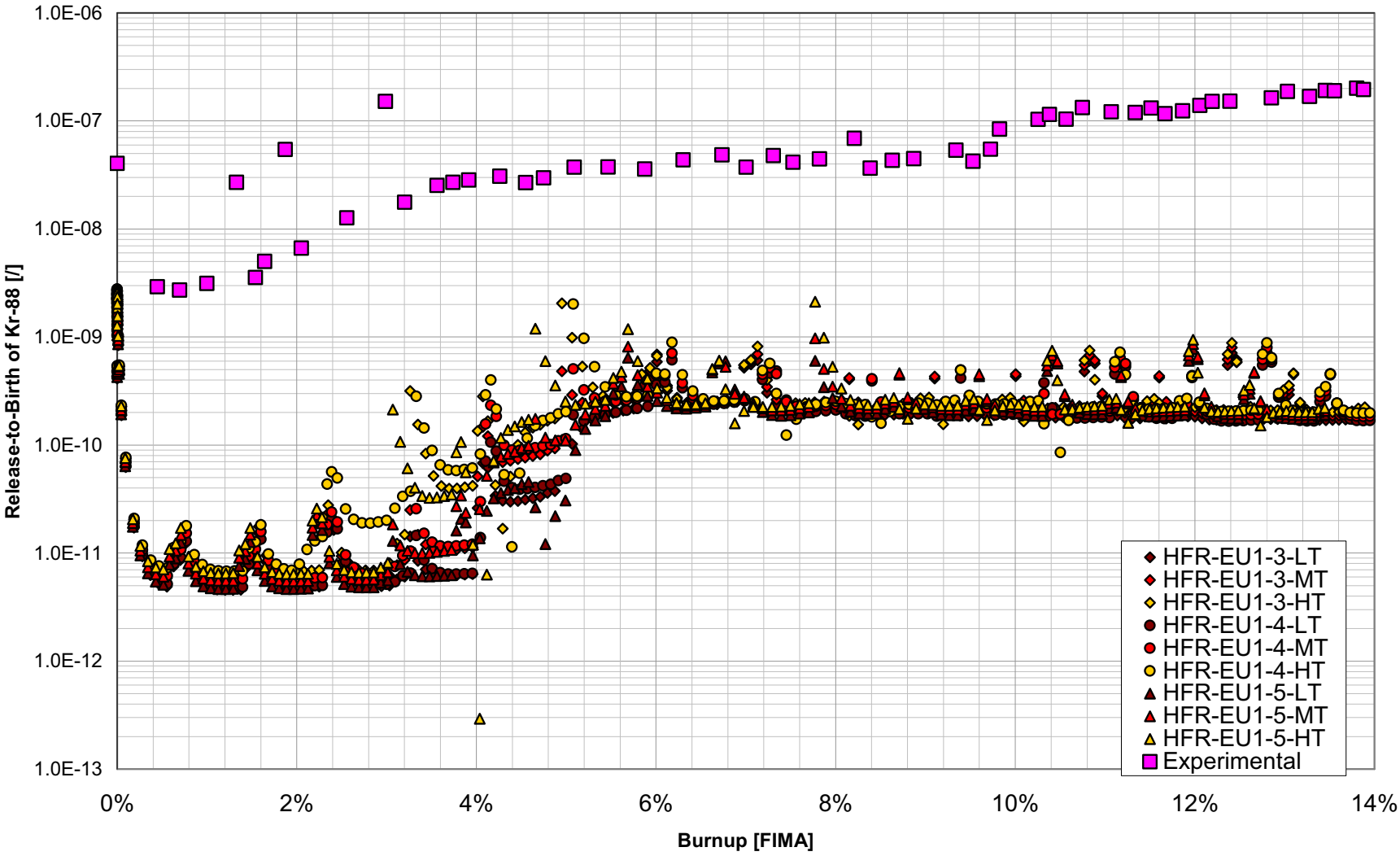

HFR-EU1-X-YY means calculation of the X pebble, with YY temperature condition (LT : Low, surface, Temperature ; MT : Mean temperature ; HT : High, center, temperature).